


# Lithological and Geomorphological Indicators of Glacial Genesis in the Upper Quaternary Strata, Nadym River Basin

Oleg Sizov<sup>1</sup>, Anna Volvakh<sup>2</sup>, Molodkov A.N.<sup>3</sup>, Andrey Vishnevskiy<sup>4</sup>, Andrey Soromotin<sup>5</sup>, and Evgeny Abakumov<sup>6</sup>

<sup>1</sup>Oil and Gas Research Institute, Russian Academy of Sciences, Moscow, Russia

<sup>2</sup>Sobolev Institute of Geology and Mineralogy, Siberian Branch of Russian Academy of Sciences, Novosibirsk, Russia

<sup>3</sup>Tallin Technological University, Tallin, Estonia 

<sup>4</sup>Novosibirsk State University, Novosibirsk, Russia

<sup>5</sup>Tyumen State University, Tyumen, Russia

<sup>6</sup>Saint-Petersburg State University, Saint Petersburg, Russia

## Abstract

Analyzing the genesis of Quaternary sediments is important for understanding the glaciation history and development of marine sediments in the northern part of Western Siberia. The problem is relevant since there is no consistent concept of the Quaternary sediments genesis in the north of Western Siberia. Their formation is associated with marine, glacial and interglacial sedimentation conditions. The research objective is to identify the persistent features characterizing the conditions of sedimentation and relief formation using the Nadym river basin as an example. The best method for studying this problem is a comprehensive analysis of the lithological, chronostratigraphic, petrographic and geomorphological studies of the Quaternary sediments upper strata. This study provides data from the analysis of the basic characteristics of quartz grains at the site. The rounding and morphology of the quartz grains provide evidence of possible glacial processing of some of the site strata. A petrographic study of selected boulder samples was performed. Some of them, by the shape and presence of [striation](#), can be attributed to glacial basins. The first use of a detailed digital elevation model applied to the study area made it possible to identify specific relief forms that could very likely be created during glaciations. Based on the analysis, we propose to consider the vast lake-alluvial plains in the Nadym river basin as periglacial regions. This idea lays the lithological framework for understanding the reasons for the formation of the modern landscape structure. The materials and descriptions provided are of interest to researchers of Quaternary sediments, topography, vegetation, and soil cover; particularly researchers engaged in revising the history of the natural environment development in the north of Western Siberia.

*Keywords: Western Siberia, paleogeography, cover glaciation, Quaternary deposits, quartz grains, petrography, DEM*

## Introduction

The history of geomorphological development in the northern part of Western Siberia was a subject of intensive discussion at the end of the 20th century. The stratigraphy of the Yenisey and Ob estuary is a key factor of the West-Siberian lowland Quaternary evolution. Numerous examples of sedimentation alternation induced by various cover glaciations of different ages and thicknesses are presented. This series of sediments was used as a background for geological interpretation of the history of West-Siberian lowland. The Q-43 national geological map of Russia for this region indicates the dominance of glacial and fluvio-glacial types of the surface sediments (Alyavdin and Mokin, 1957). The possible existence of ice sheets and related permafrost sediments was identified as a key issue at the beginning of

50 the systematic geological study of the [north of West Siberia](#) in the 1960s. Some  
51 researchers (e.g., Svendsen et al., 2004) suggested that there were extensive  
52 glaciations that resulted in blocking [the Ob, Yenisei, Pur, Taz, Nadym rivers](#)  
53 at certain stages, leading to the formation of large glacier dammed lakes (Grosvald,  
54 1999).

55 Another point of view considers possible glaciation on the plain (e.g.,  
56 Generalov, 1986). It explains why the landforms are a sequence of terraces formed  
57 by marine transgressions of various ages. There is also an opinion that the glaciation  
58 was localized in the form of ice caps on separate watersheds and that the river flows  
59 of the [Ob, Yenisei, and other rivers](#) were unblocked (Velichko, 1987; Velichko et  
60 al., 1997). Bolshiyarov (2006) challenged this opinion and introduced the “passive  
61 glaciation” concept. In this context, it is assumed that the sea level fluctuations might  
62 have created extensive abrasion platforms. Another viewpoint suggests that the  
63 forms of relief which previously were considered as glacial and fluvioglacial  
64 (moraines and eskers), did not originate from cover glaciations, but resulted from  
65 erosion, abrasion, and thermokarst outcrops associated with permafrost-erosion and  
66 tectonic processes of the late Pleistocene. It was suggested that isolated parts of  
67 Smarovskoye glaciation ([300,000 to 230,000 years ago](#)) existed in some areas of the  
68 Tyumen region combined with relics of ancient marine terraces (Lazukov, 1972).  
69 Later, there was a heated discussion in the Russian geology community regarding  
70 the nature of possible glaciations and sedimentation history of Western Siberia. It  
71 was suggested that glaciations extended up to Siberian Uvaly that continued as the  
72 ancient periglacial Mansyiskoye lake (Grosvald, 1999). Bolshiyarov (2006)  
73 suggested that the glaciations were passive, without forming a discontinuous cover  
74 or preferential flow blocking in the area topography. At the same time, the abrasion  
75 relief with extended ledges was formed in the late Pleistocene period. Finally, the  
76 Q-42-43 national geological map [indicates](#) that there is a combination of both  
77 terrestrial glacial and marine glacial sediments and numerous lake terraces in  
78 Western Siberia (Babushkin, 1996). Nowadays, the glacial sediments are excluded  
79 from the current version of the national geological map (Faibusovich and  
80 Abakumova, 2015) which contradicts the results obtained by Fredin et al. (2012) and  
81 Astakhov et al. (2016). Currently, there is no uniform concept of the landforms  
82 genesis in Western Siberia. The basing of the Nadym River is considered as most  
83 important for the Quaternary interpretation of the local Pleistocene history. The  
84 topography and sediments of the Nadym River provide the most information for the  
85 study of glacial landforms. Many field investigations and remote sensing operations  
86 were completed by multiple generations of researchers, providing a valuable  
87 baseline for future studies. The results of studying the Nadym River and adjacent  
88 areas, combined with other data, served as a basis for a classification of the  
89 Quaternary deposits in West Siberia (Maslennikov, 1998; Sedov et al, 2016;  
90 Sheinkman et al, 2016; Rusakov et al, 2018). Nevertheless, the current geological  
91 map (Faibusovich and Abakumova, 2015) still has unsolved issues that are  
92 highlighted as new geological and [geomorphological](#) data are obtained.

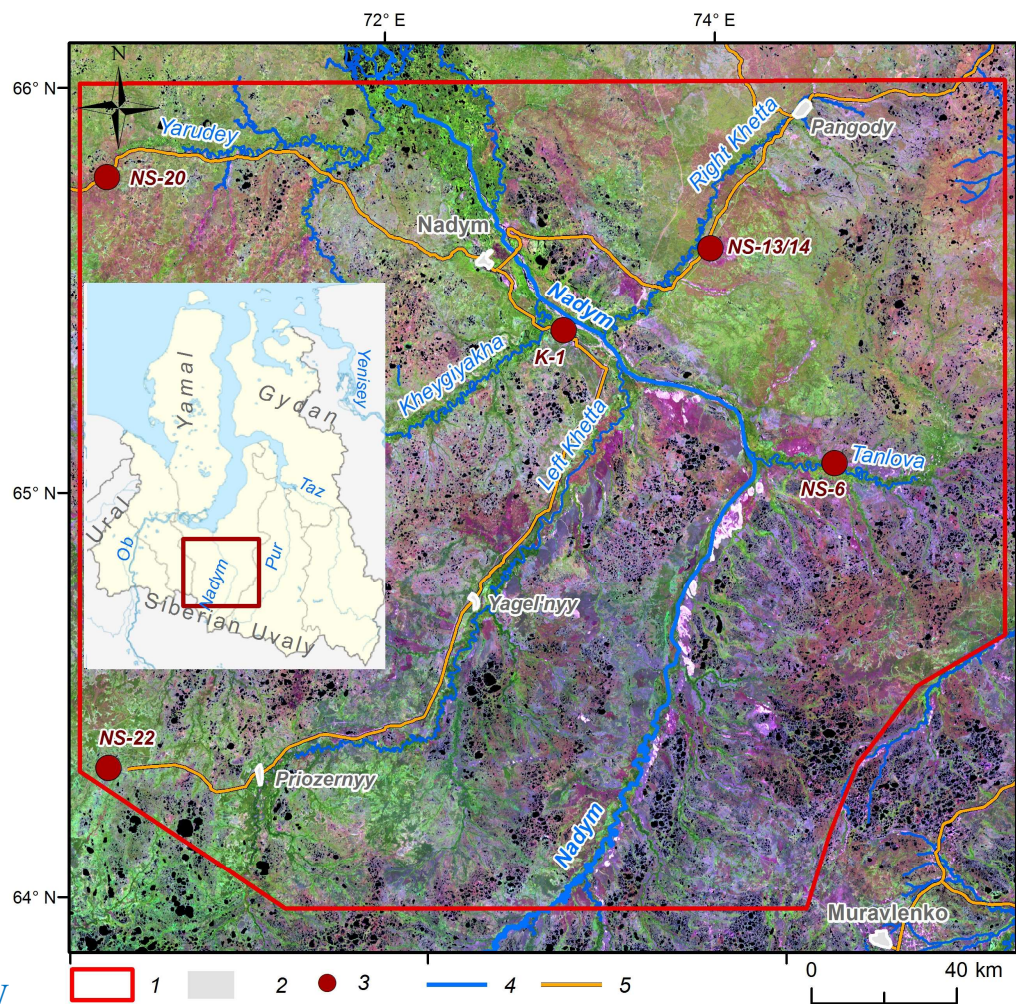
93 The study objective is to summarize the results of detailed lithological,  
94 chronostratigraphic, petrographic and geomorphological studies conducted in the

95 Nadym River basin, and to identify the origins of the key factors of sedimentation  
96 accumulation and topography.

97

### 98 **Materials and Methods**

99 Fieldwork was conducted in 2016-2018 in the Nadym River Basin, including  
100 the valleys of its main tributaries: **Kheygiyaha, Yarudey, Tanlova, Left and Right**  
101 **Khetta**. The region is characterized by a moderate human-induced burden. There are  
102 main gas pipelines (Urengoy-Pomara-Uzhhorod, Nadym-Punga-Lower Tura, etc.),  
103 high-voltage power transmission lines (200, 500 kV), an pipeline from **Yarudeyskoe**  
104 **oilfield** and the Nadym-Prizernyy road. The survey covered the natural exposures  
105 along riverbanks, walls of dry quarries located at the watersheds and river terraces  
106 as the most informative terrain features. **This paper is based on the results of detailed**  
107 **studies of the five most prominent stratigraphy sections of the upper part of**  
108 **Quaternary sediments (Figure 1). For clarity, the section coordinates, their locations,**  
109 **survey dates and the total thickness of the studied deposits are specified (Table 1).**  
110



111

NEW

112

112 Fig. 1. Overview map: 1: study area; 2: settlements; 3: studied and sampled locations; 4:  
113 waterways; 5: roads. Background image: Landsat 8, 2000.

114

115

Table 1

116

Site Properties

N	Coordinates N, E	Top of section elevation, m a.s.l.	Geogenic location	Sampling point location	Survey date	Thickness, m
K-1	65.351044 72.974041	24	Second above flood plain terrace	Wall of quarry	21.08.2016	4.2
NS-6	64.974808 74.499714	44	Second above flood plain terrace	River break	18.08.2017	9.5
NS - 13/14	65.52992 73.875985	44,5	Kamiform hill	Top and slope of hill	22.08.2017	5.1
NS-20	65.778072 70.29182	57	Esker sediments	Wall of quarry	11.08.2018	16
NS-22	64.31688 70.232456	130	Watershed	Wall of quarry	13.08.2018	1.5

117

118

119

120

121

122

123

124

125

126

127

128

129

130

131

132

133

134

135

136

137

138

139

140

141

142

143

144

145

146

147

148

Samples for bulk chemical composition, grain size distribution, sand quartz grain morphoscopy and morphometry, as well as luminescent analysis of sandy textured particles of feldspars were taken from each specified layer of the studied sections in order to clarify the conditions of the sediment formation.

The bulk content of oxides was determined by the X-ray fluorescence method at the Analytical Center for Multi-Elemental and Isotope Research, Siberian Branch (SB), Russian Academy of Sciences (RAS), Novosibirsk, Russia, and at the laboratory of the Institute for Physical, Chemical and Biological Problems of Soil Science (Pushchino, Russia). The grain size distribution was determined by conventional fractions separation (sieve analysis) of samples with the Fritsch Analysette 3 vibratory sieve shaker. The fractions were weighed with laboratory scales, 0.1 g accuracy. 17 samples from the sections NS-6 and NS-13/14 were analyzed at the Laboratory of Ground Mechanics, Institute of Cryosphere of the Earth, Tyumen Research Center RAS with the Mastersizer 3000E laser diffraction particle size analyzer (Malvern Panalytical, Britain). Since different laboratories measured the granulometric composition, the figures for the lightest fractions are slightly different.

The Altami CM0870-T binocular microscope was used to study the quartz grains (50 grains per sample) taken from the coarse sand fraction. The grain surface morphology was studied with the JEOL JSM-6510LV scanning electron microscope (SEM) using the secondary electron image (SEI) at the Analytical Center for Multi-Elemental and Isotope Research, SB, RAS. According to the technique applied (Velichko and Timireva, 1995), the grain scale was determined using Rukhin (1969, Figure 2) and Khabakov (1946), where 0 is an angular, and IV is a perfectly rounded grain. The coefficients scale of roundness and the grades of dullness (Velichko and Timireva, 1995) were estimated for each sample. The dullness of the grains was determined visually as glossy (shiny), quarter-matte, half-matte, and matte. The grain surface microrelief structure study was based on numerous published diagnostic features found in grains with various genesis and sediment accumulation conditions (e.g. Velichko and Timireva, 1995; Krinsley, Doornkamp, 2011; Vos et al., 2014; Woronko, 2016; Kalinska-Nartisa et al., 2017). The previous studies in

149 Western Siberia that examined sand quartz grain micromorphology covered peat  
150 histic sand deposits in the area of Siberian Uvaly, valleys of the rivers Taz and Pur  
151 (Velichko et al., 2011) and aeolian sediments of the southern part of Western Siberia  
152 (e.g. Sizikova and Zykina, 2015).  
153

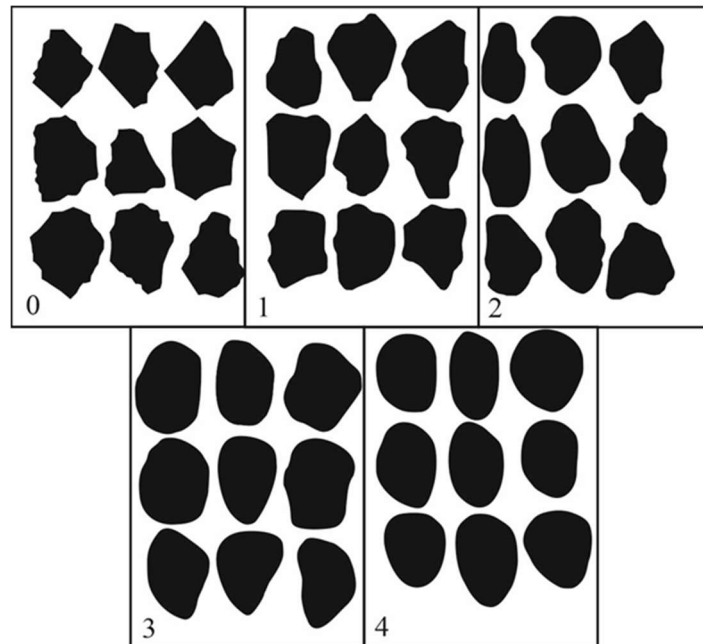


Fig. 2. Pattern (Rukhin, 1969)

0, 1, 2, 3, 4 are the classes of roundness (Khabakov, 1946)

154  
155  
156  
157

158 The potassium feldspar-based infrared optically-stimulated luminescence (IR-  
159 OSL) dating method was applied to produce an absolute chronology of the deposits  
160 from the five sections studied in the present work. The upper limit of the method is  
161 normally 300–500 ka, depending on burial conditions and the physical properties of  
162 the mineral. The reliability of the dating technique used in the present study is  
163 demonstrated by comparative results obtained using several numerical dating  
164 methods (mollusc shell-based electron spin resonance (ESR), quartz-based optically  
165 stimulated afterglow (OSA), U-Th and  $^{14}\text{C}$ ) applied to the same sedimentary samples  
166 (Molodkov, 2012). An overview of the IR-OSL dating procedure is presented by  
167 Molodkov and Bitinas (2006). All IR-OSL ages reported in this paper were obtained  
168 in the Research Laboratory for Quaternary Geochronology, Institute of Geology,  
169 Tallinn University of Technology.

170 In addition to the analysis at the sampling area, samples were taken for  
171 petrographic examination. The samples were cut perpendicular to the bedding  
172 direction (if any) and made into transparent sections. The Carl Zeiss AxioScope A1  
173 optical microscope at the Geology and Mineralogy Institute, SB RAS (Novosibirsk)  
174 was used.

175 For the first time for the studied area, digital terrain models (DTM) with  
176 spatial resolution of 12 and 26 m/px based on TerraSAR -X and TanDEM -X radar  
177 data were used to characterize the geomorphological structure. The mapping is based  
178 on the remote features available in the literature (Atkinson et al., 2014; Astakhov et  
179 al., 2016, etc.) and the comparison of the field and remote sensing data (Table 2). In

180 addition, public multi-spectrum space images from Sentinel-2 (10 m/px.) were used  
 181 to clarify the location of such natural features as rivers, lakes, swamps, and forests  
 182 (<https://scihub.copernicus.eu/>).

183  
 184  
 185

Table 2  
 Remotely sensed features of glacial and fluvio-glacial relief

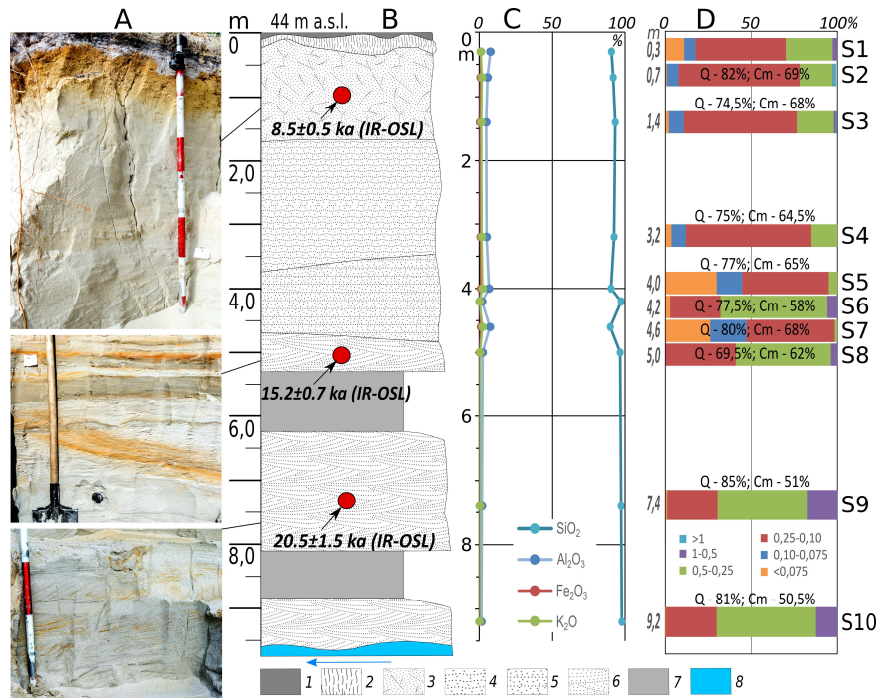
Relief features	Remotely sensed features
Kame-like hummocks	Irregularly scattered hills and ridges with their relative elevation not exceeding 10-20 m. The hills have plateau-like summit, the slopes are gently convex, the slopness varies. The hills and ridges are easily identified on the DTM against the flattened background; often they are separated by no-outflow basins and hollows. The hills are at the highest parts of the watersheds and often from groups or even curved chains oriented NE to SW, or E to W. Sparse vegetation areas are associated with the highest parts of the hills.
End moraines	Mostly associated with the watersheds. They are narrow, tortuous upheavals (relative elevation is up to 5-7 m, sometimes to 10 m). The survival rate varies. They can be in the form of high linear upheavals with steep slopes to low kettlebacks 10-12 km long. With high resolution DTMs (2-10 m), the small local boundary moraine formations are easily identified; for mid-resolution DTMs (25-30 m) the large features with a low survival rate are identified. The key properties are the length and the position: the flat moraine pattern usually forms an interconnected structure that reflects the ice sheet extents and the stages of its degradation.
Parallel ridges	As opposed to the terminal moraine ridges, the linear ridges are smaller and shorter while their direction is more pronounced (almost no bends.) When ridges are poorly expressed, an additional indicator is a linear structure of the multispectral image caused by the similar orientation of the river valleys, chains of small lakes, forest and bog boundaries..
Valley trains	Twisted similarly to smooth river meanders. Nowadays they are swamped and turned into lakes. Merging and splitting, they form a typical pattern of the hydrographic network. The valleys are often associated with expected drainwater sources mostly located in glacial accumulative formations on the watersheds. The valleys often terminate with chains of lakes perfectly visible in satellite images.

186  
 187  
 188  
 189  
 190  
 191  
 192  
 193

## ***Results***

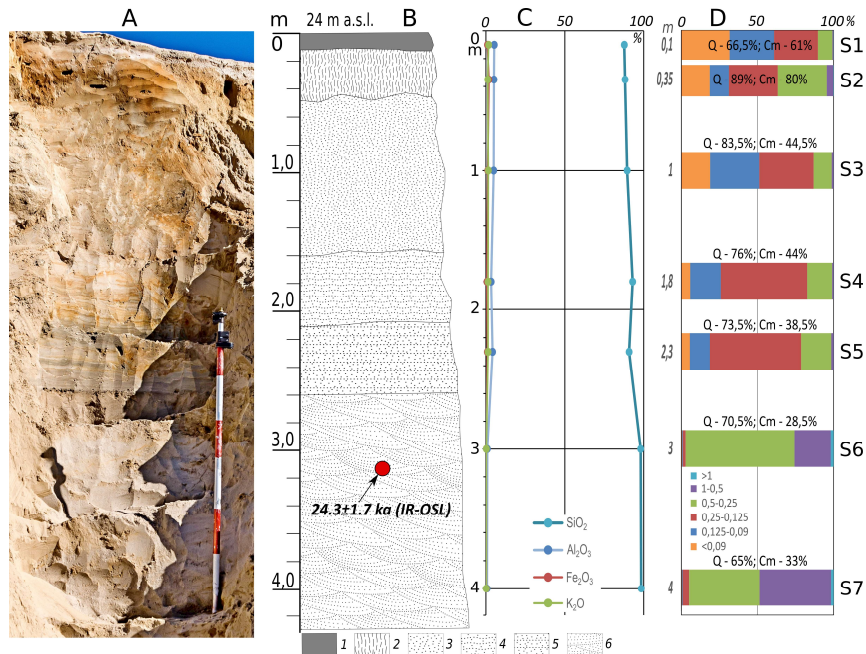
### ***Characteristics of the Sections***

The summary results of the Quaternary sediment section study are shown in Figures 3-7 and Annexes 1, 2. From the data obtained, the following characteristic conditions of sediment accumulation can be distinguished:



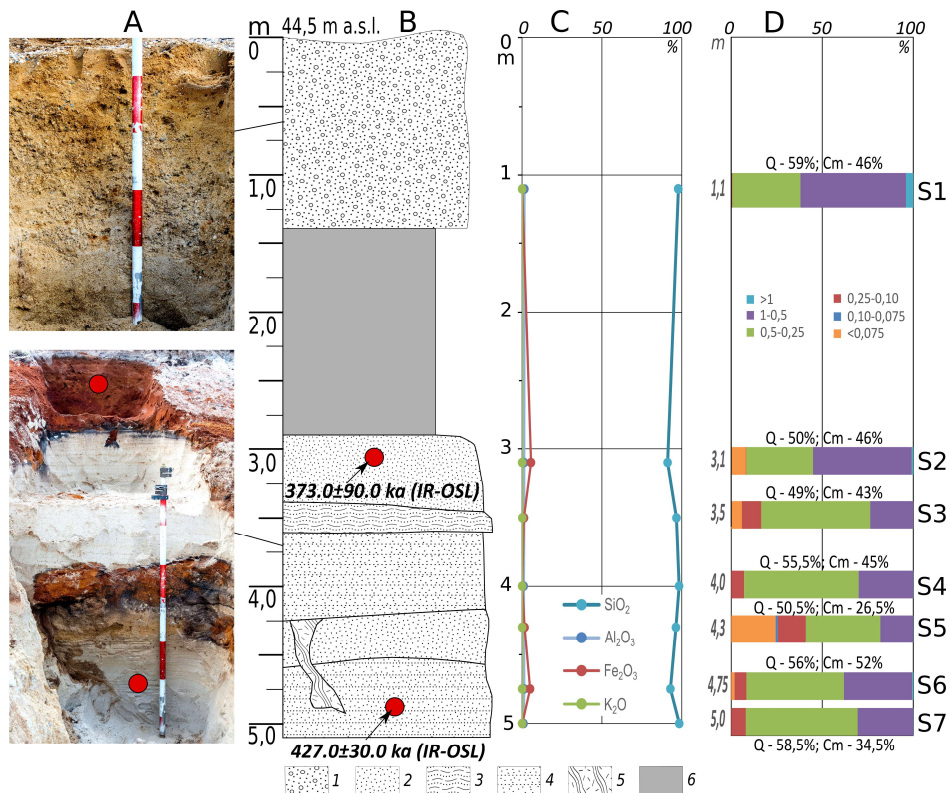
194  
195  
196  
197  
198  
199  
200  
201  
202

Fig. 3. Summary results of research for section NS-6. A: photographs (by Sizov in 2017); B: geological structure and the dating results (refer to Table 3); C: bulk chemical data; D: grain size distribution (fractions, mm). Symbols: 1: podzol horizon of modern soil; 2: illivial-iron (spodic) horizon of modern soil; 3: sands without stratification; 4: undulating sand with secondary ironing; 5: horizontally layered sand with stratification of loam; 6: medium-and coarse-grained oblique sand; 7: colluvium; 8: river level; Q: coefficient of roundness of the sand quartz grains; Cm: degree of dullness; S: sample number.



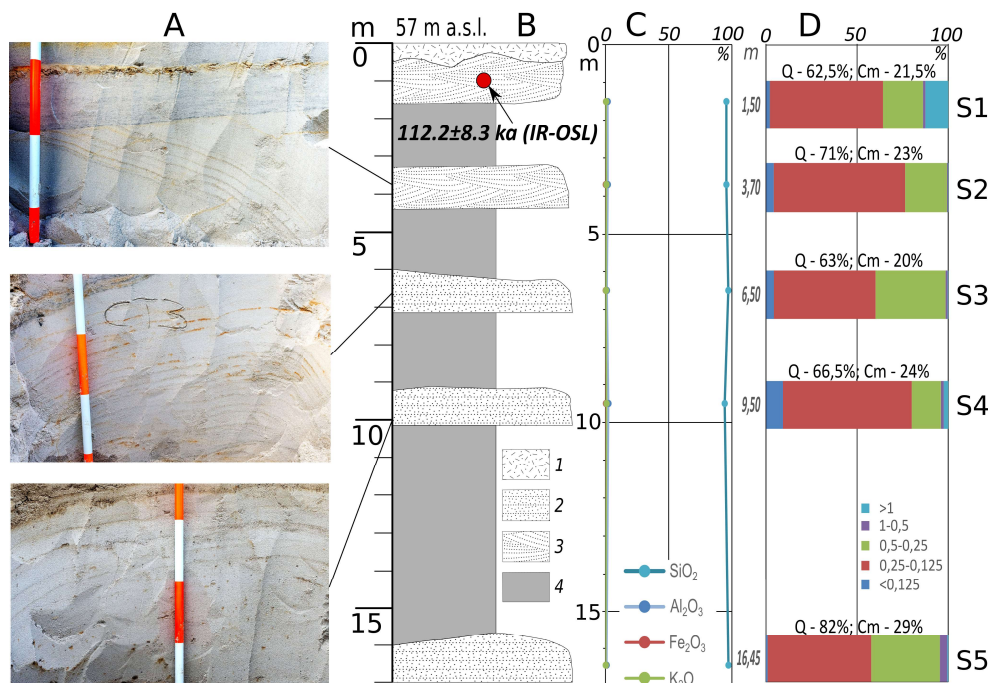
203  
204  
205  
206  
207  
208  
209  
210  
211

Fig. 4. Summary results of research for section K-I: A: photographs (by Sizov in 2016); B: geological structure and the dating results (refer to Table 3); C: bulk chemical data; D: grain size distribution (fractions, mm). Symbols: 1: podzol horizon of modern soil; 2: illivial-iron (spodic) horizon of modern soil; 3: sands without stratification; 4: undulating sand with secondary ironing; 5: horizontally layered sand with stratification of loam; 6: medium-and coarse-grained oblique sand; 7: colluvium; 8: river level; Q: coefficient of roundness of the sand quartz grains; Cm: degree of dullness; S: sample number.



212  
213  
214  
215  
216  
217  
218  
219

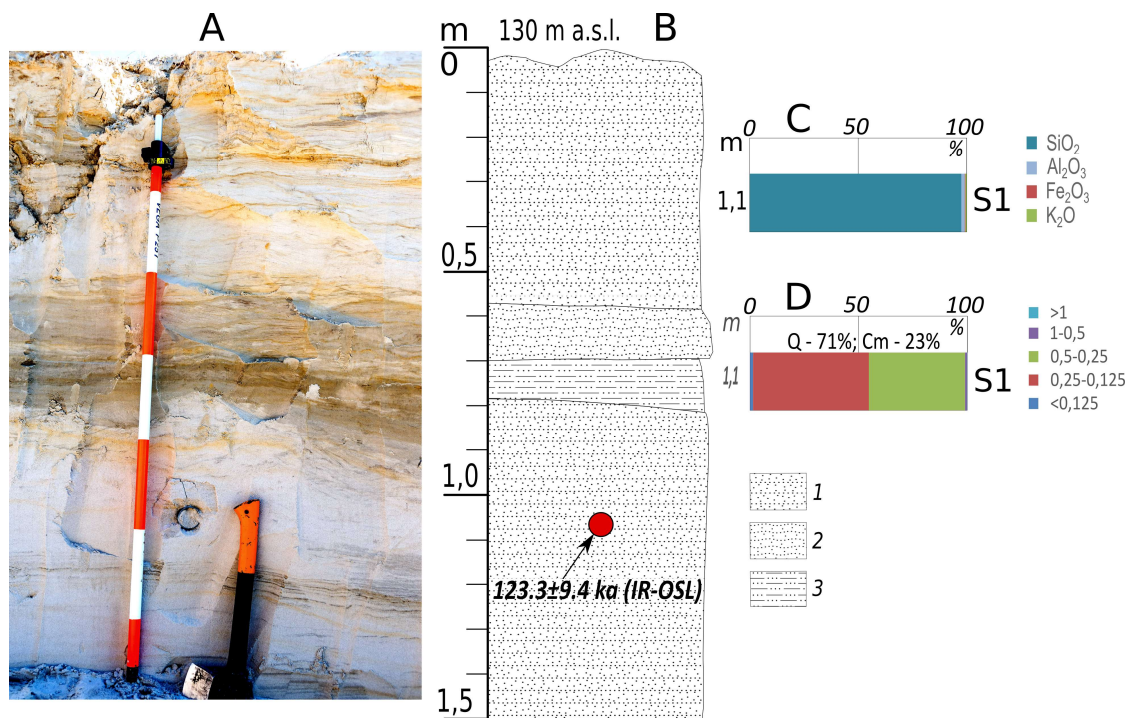
Fig. 5. Summary results of research for section NS-13/14: A: photographs (by Sizov in 2017); B: geological structure and the dating results (refer to Table 3); C: bulk chemical data; D: grain size distribution (fractions, mm). Symbols: 1: coarse sand with pebbles; 2: unstratified red sand; 3: undulating black sand; 4: horizontally layered sand; 5: wedge filled by deposits of the overlying layer; 6: colluvium; Q: coefficient of roundness of the sand quartz grain; Cm: degree of dullness; S: sample number.



220  
221  
222  
223  
224  
225  
226

Fig. 6. Summary results of research for section NS-20: A: photographs (by Sizov in 2018); B: geological structure and the dating results (refer to Table 3); C: bulk chemical data; D: grain size distribution (fractions, mm). Symbols: 1: overburden; 2: horizontally layered sand; 3: medium- and coarse-grained oblique sand; 4: colluvium; Q: coefficient of roundness of the sand quartz grains; Cm: degree of dullness; S: sample number.





227  
228  
229 *Fig. 7. Summary results of research for section NS-22: A: photographs (by Sizov in*  
230 *2018); B: geological structure and the dating results (refer to Table 3); C: bulk chemical data;*  
231 *D: grain size distribution (fractions, mm). Symbols: 1: horizontally layered grey sand; 2: oblique*  
232 *layered sand; 3: horizontally layered sandy loam; Q: coefficient of roundness of the sand quartz*  
233 *grain; Cm: degree of dullness; S: sample number.*

234 1. Alluvial deposits predominate at the lower geomorphological level (up to  
235 40-45 m.). Sections K-1 and NS-6 show the similar structure of the second above-  
236 ground terrace of the Nadym and Tanlov rivers: in the upper part, thick podzolized  
237 soil is formed over the aeolian deposits; in the middle part, floodplain type deposits  
238 dominate; and in the lower part they are replaced by well-leached gray layered sand.  
239 Down the profile, the SiO<sub>2</sub> content increases, while the content of other chemical  
240 elements is low. The middle part of the section is dominated by fine and medium-  
241 grained sand, the portion of large fractions increases in the lower part where single  
242 pebbles with diameters up to 3-4 cm are found. There are no permafrost-affected  
243 sediments.

244 2. At the middle **topographical** level, the sections show the structure of a NS-  
245 13/14 kamiform hill and a linear-oriented relief (NS-20). The top of the hill is  
246 covered with a solid layer of pebbles; at 1.2 m depth, it is followed by coarse sand.  
247 Sandy deposits forming two distinct cycles are exposed in the middle part of the hill.  
248 The unbroken red-colored sand is followed by black sand with slightly horizontal  
249 orientation, which in turn is followed by light-grayish horizontally layered sand. In  
250 the lower profile, the cycle is repeated; the difference is that the layer of intensively  
251 reddish sand is not as thick. In the left lower part of the section, there is a frost wedge  
252 microdepression, filled **with the overlying layer sediments**. In general, the section is  
253 dominated by medium- and coarse-grained sands of monomineral composition (the  
254 shares of Fe, Al and other chemical elements are insignificant).

255 In section NS-20, the slope of the extended elevation is exposed. It is  
256 composed of a monotonic body of grey monomineral parallel and oblique-oriented

257 quartz sand. The sands throughout the section have an identical grey color and fine-  
 258 grained composition. The presence of thin iron-containing layers does not affect the  
 259 chemical composition of sediments: SiO<sub>2</sub> prevails in all layers. Local hills up to 5-8  
 260 m high covered with large pebbles and boulders on the surface were found on the  
 261 top of the ridge along the survey path. In an exploration ditch on the top of the  
 262 microhill (1.5 m deep), large-grained, **non-laminated** sandy sediment with the  
 263 abundance of **angular** pebbles, gravel, and single large (diameter up to 30-40 cm)  
 264 boulders were exposed. Their structure is similar to the deposits of the upper part of  
 265 section NS-13/14. In none of sections, permafrost sediments or traces of frost  
 266 cracking occur.

267 3. The NS-22 is at the upper watershed in a small quarry. The quarry exposes  
 268 sandy and sandy-loam bedded deposits of the large hill on the upper topographical  
 269 level. Sands in the sample are grey-colored, fine and medium-grained. The SiO<sub>2</sub>  
 270 content is 96.49%. A huge number of large, weakly rounded boulders, diameter up  
 271 to 1.5 m in size, was found in the quarry and on the sandbank of the nearest lake  
 272 (100-200 m from the quarry).

273 It should be noted that grey fine, medium- and coarse-grained sands of  
 274 monomineral quartz composition are present in all sections (except for NS-13/14).  
 275 In river terraces, such sands have oblique lamination, while on the watershed **they**  
 276 **are oriented** horizontally. The sands have no permafrost features, cracking traces  
 277 and, in general, poor chemical composition. A landscape vegetation feature of such  
 278 sediments is pine sparse forests, which are able to grow on poor sandy soils with a  
 279 well-drained hydrologic behavior. Sandy soils lack organic materials and debris of  
 280 fossil clams, and do not show any salt content. Despite the presence of large debris  
 281 on the scree slopes; boulders do not occur directly in the sands. Based on  
 282 morphological, particle size and chemical features infer we infer that this type of  
 283 sand sediment could be formed in subaquatic conditions in more severe  
 284 environments as compared to modern climatic conditions. This is also confirmed by  
 285 correlation coefficient value – quartz content is negative correlated with key oxides  
 286 in bulk composition of the fine earth (Annex 2).

287

### 288 3.2. Sediments Dating Results

289 IR-OSL ages for the sediment samples from the sites studied and the related  
 290 analytical data are listed in Table 3.

291

292

293

Table 3  
 Absolute dating by the IR-OSL method

Section	Sampling depth (m)	Sample code	Age (ka)	U (ppm)	Th (ppm)	K (%)
K	3.15	RLQG 2443-057	24.3 ± 1.7	0.11	0.45	0.01
NS-6	1.0	RLQG 2563-019	8.5 ± 0.5	0.79	0.73	0.94
NS-6	5.0	RLQG 2564-118	15.2 ± 0.7	0.01	0.00	0.14
NS-6	7.3	RLQG 2565-118	20.5 ± 1.5	0.01	0.00	0.14
NS-13/14	3.1	RLQG 2567-019	373.0 ± 90.0	0.00	0.00	0.00
NS-13/14	4.9	RLQG 2568-019	427.0 ± 30.0	0.35	0.74	0.00
NS-20	1.1	RLQG 2577-059	112.2 ± 8.3	0.96	4.19	0.34

NS-22	1.0	RLQG 2578-059	123.3 ± 9.4	1.29	2.00	1.31
-------	-----	---------------	-------------	------	------	------

294

295 From section K-1, a single date of 24.3±1.7 (RLQG 2443-057) was obtained  
 296 at the depth of 3.2 m. According to this age, [sediment deposition](#) took place at the  
 297 very end of the third (Lipovka-Novoselovo) warm phase, which was recorded in the  
 298 north of Western Siberia during MIS 3 (Marine Isotope Stage 3) by both the <sup>14</sup>C  
 299 (Kind, 1974) and clam shell-based ESR (Molodkov, 2020) methods.

300 The normal sequence of the youngest ages of 20.5 ka (RLQG 2565-118), 15.2  
 301 ka (RLQG 2564-118), and 8.5 ka ([RLQG 2563-019](#)) was obtained for section NS-6  
 302 at the depths of 7.3 m, [5.0 m](#), and [1.0 m](#), respectively. Specific analytical features  
 303 suggest the supply of the sedimentary rock from the same source area. The genesis  
 304 of the deposits is also identical. It implies similar conditions for the rock transfer  
 305 despite the likely difference in climatic conditions.

306 Somewhat unexpected were the dating results for two consecutive layers in  
 307 section NS-13/14: 427.0 ka ([RLQG 2568-019](#)) and 373.0 ka ([RLQG 2567-019](#)).  
 308 Finding very old Pleistocene deposits (MIS 11) is exceedingly rare. Judging from  
 309 the analytics, the sedimentary rock in these layers came from different source areas  
 310 and has fluvial, most likely river genesis. Under the given conditions of burial and  
 311 physical properties of the mineral, the upper dating limit may be at least three times  
 312 higher (i.e., up to about a million years).

313 The last two datings at 123.3 ka ([RLQG 2578-059](#)) and 112.2 ka  
 314 ([RLQG 2577-059](#)) were obtained from two sections: NS-22 and NS-20,  
 315 respectively. [Their](#) common feature is that both of them fall into MIS 5, as well as  
 316 the fact that the corresponding sedimentary rock also came from various source  
 317 areas. The studied sediments on the base of a group of key features are supposed to  
 318 have fluvial (river and lake) origin.

319

### 320 *3.3. Sand Quartz Grain Morphoscopy and Morphometry.*

321 Refer to Annexes 4-13 for the key results: coefficient of roundness, degrees  
 322 of dullness, and examples of the quartz grain appearance. The following is a brief  
 323 description of the main features.

324 NS-6. Aeolian genetic group. The upper part of the section (samples S2 and  
 325 S3) is characterized by a high coefficient of roundness (Q; 74.5 - 82%) and degree  
 326 of matting (Cm; 68 - 69%). IV rounding class matte grains prevail; the complete  
 327 grain distribution vs. rounding and surface dullness are shown in Annex 4. The most  
 328 common element of grains microrelief in the S1 sample is a micro-pitted surface  
 329 (Annex 9 a, b), which is a feature of aeolian transportation (Velichko and Timireva,  
 330 1995). Chemical etching is sometimes found in depressions. High coefficients of  
 331 roundness (Q) and degrees of dullness (Cm) along with the predominance of micro-  
 332 pitted grain texture suggest the dominance of aeolian processes during the  
 333 sedimentation. Several grains show signs of subaquatic treatment and origin in the  
 334 form of crescentic depressions and V-shapes percussions (Annexes 9 a, b), which  
 335 preceded the aeolian stage. It seems to be associated with the accumulation of rock  
 336 from the river valleys.

337 For quartz grains from the floodplain deposits (samples S4-S8), the rounding  
338 coefficient (Q) is within the range of 65-80%; the degree of dullness (Cm) is 58-  
339 68% (Figure 3). On average, IV rounding class grains (Refer to Annex 4) with a  
340 half-matte surface prevail in the samples. The number of completely glossy grains  
341 increases (up to 22%). The entire grain surfaces have signs of subaquatic processing:  
342 V-shaped percussions (Annex 9 d), often forming a fine-pitted surface (Annex 9 c,  
343 d), and separate crescent gouges. Many grains show traces of aeolian treatment,  
344 expressed as a micro-pitted texture (Annex 9 c), which corresponds well to a  
345 sufficiently large share of matte grains in the sample. It can be assumed that deposits  
346 of this layer are formed by fluvial river and aeolian processes in the coastal  
347 environment.

348 For samples from the lower part of the section (samples S9, S10) Q = 81-85%  
349 and Cm is 50.5-51%. Most grains belong to the IV rounding class. The number of  
350 glossy grains (up to 32%) is significantly higher than in overlying sediments (Annex  
351 4). The primary grain treatment traces on the surface of all grains, regardless of the  
352 roundness and dullness, are fine-pitted surfaces (Annex 9 e, f) and individual well-  
353 developed V-shaped microdepressions (Annex 9 f), which is a sign of active river  
354 fluvial transportation. There are grains of the II and III classes of roundness; they  
355 differ from most grains by the presence of flat faces (Annex 9 g, h). The shapes of  
356 these grains resulted from the previous stages of grain treatment. There are also signs  
357 of aquatic treatment on its surfaces (Annex 9 g, h).

358 The K-1 grain distribution across the section [matches](#) well the morphometric  
359 and morphological properties of the NS-6 section (see Annex 5 for the grain  
360 distribution by roundness and dullness). Samples S6-S7 lying in the base of the  
361 section provides important information. These samples differ in grain morphology  
362 from overlying sediments. They are characterized by the lowest cross-sectional  
363 values of the coefficient of roundness (63-65%) and the degree of matting (33-35%),  
364 the presence of glossy grains in all classes of roundness (Annex 10), constrained or  
365 ground flat faces at grains, and the development of sickle-like texture and fine pits  
366 on the grain surface. With these features, it can be concluded that this layer was  
367 formed by fluvial processes, but it should be emphasized that there is a rock in its  
368 composition that may have been exposed to glacial processes in the past.

369 NS-13/14. For S1 deposits Q= 59% and Cm = 46%. Angular grains, class I  
370 (32%) and medium-rounded grains, class II (24%) predominate. Most grains have  
371 half-matte (34%) and quarter-matte (32%) surface (Annex 6). The grains can be  
372 categorized into two groups. The first group is represented by well-rounded mature  
373 grains with a ubiquitous fine-pitted surface (Annex 11 a), which is a sign of  
374 treatment by aqueous streams. In the second group, there are grains of irregular  
375 shape (Annex 11 b), often with multiple or conchoidal fractures. The faces have  
376 traces of treatment in subaquatic environment. Grains of the second group show  
377 separate V-shaped and rarely crescentic-shaped percussions; their number and  
378 location indicate a lower exposure to water flow. The presence of these two different  
379 groups of grains suggests the ingress of rock from different sources of the rock. [One](#)  
380 [one them could be the subangular fluvioglacial deposits.](#)

381 For underlying deposits (S2-S7) Q=49 – 58.5% and Cm=26.5-52%. There,  
382 poorly-rounded and middle-rounded grains of classes I and II with a glossy or  
383 quarter-matte surface prevail (Annex 6). The grain surface is dominated by traces of  
384 low-activity subaquatic treatment: V-shaped and crescentic microdepressions  
385 (Annex 11 c-h). Irregular grains with smooth surfaces are most common, often with  
386 fractures (Annex 11 e, f, h), which probably indicates its arrival from a source with  
387 poorly rounded materials. There are grains with conchoidal fractures formed by  
388 desquamation processes due to grain freezing (Velichko and Timireva, 1995) or  
389 under a big pressure applied to the grain (Immonen et al., 2014; Vos et al., 2014.)  
390 There are also V-shaped percussions along its surface, suggesting that the  
391 deformation occurred before the last fluvial treatment. Many grains were highly  
392 exposed to chemical processes expressed as etching through the depressions on the  
393 grain and the Fe-Mn skins. The development of V-shaped forms only along the  
394 protruding parts of the grain, a well-developed crescentic-shaped texture and non-  
395 ubiquitous fine-pits, the average values of the coefficient of roundness and low  
396 degrees of maturation suggest that the final processing of grains occurred in a  
397 relatively calm aquatic environment. For S2 and S3 samples, in addition to traces of  
398 subaquatic treatment, there are grains with small micro-pits (Annex 11 c, d), a sign  
399 of aeolian treatment of grains.

400 NS-20. For samples S1-S5, the coefficient of roundness (Q) is in the range of  
401 62.5-82% and the degree of dullness (Cm) is 20-29%. Glossy grains of II and III  
402 classes of roundness prevail (Annex 7). In the most most sediments (S1), there are  
403 signs of aeolian treatment of grains expressed as micro-pits (Annex 12 a, b).  
404 However, they have a rather low value of Cm, which is not typical of aeolian  
405 deposits. This suggests that the local aeolian redeposition of underlying sediments  
406 occurred. The underlying layers (S2-S5) have sediment features; their formation is  
407 probably associated with fluvio-glacial processes: the surface of most grains is highly  
408 uneven, cavernous, and strongly mechanically deformed. These properties can be  
409 found in glacial conditions (at the stages of previous processing). This is also  
410 suggested by the presence of deep-pits, grooves and parallel scratches of various  
411 configurations (Annex 12 c, d, h). The last agent in their treatment was a subaquatic  
412 process, as indicated by frequently occurring V-shaped and crescentic depressions  
413 (Annex 12 e, f, g).

414 NS-22. The coefficient of roundness (Q) is 79% and the degree of dullness  
415 (Cm) is 31%. Most of the grains belong to class III of roundness, a slightly smaller  
416 number of grains are of class IV; glossy grains prevail (Annex 8). The morphology  
417 of the grain surface is quite uniform and is mainly represented by grains with fine  
418 pits covering the grain surface almost completely (Annex 13 a-f) or developed only  
419 on microelevation parts of the grain (Annex 13 e, f). This surface is a characteristic  
420 feature of the long-term grain processing in a sufficiently active subaquatic  
421 environment.

422  
423

### 3.4. Petrography

424 The petrographic analysis of 15 samples taken in a quarry nearby the section  
425 AS-3 (Figure 8, coordinates: N65.061417°, E72.943848°) enabled to distinguish  
426 several groups of materials:

427 1) The first group (6 samples) is presented by grey, yellowish-grey, and  
428 greenish-grey fine-grained and very fine-grained sandstone and siltstone with slab  
429 jointing. They are usually moderately or poorly sorted and have primary foliation  
430 that is emphasized by the regular orientation of flattened grains, varying grain size,  
431 and matrix content. The matrix is hydromicaceous clay, sometimes with ferruginous  
432 cement, with a small portion of silica. The fragments are usually sub-rounded or sub-  
433 angular. The rock is composed of polymictic sandstones, similar to arkoses  
434 sandstones. Quartz and feldspar prevail among the mineral grains, composing ~30  
435 vol% of the fragments, while another third is predominantly composed of siliceous  
436 rock fragments. Some samples contain significant amounts of muscovite (up to 5%  
437 by volume), chlorite (including pseudomorphs after the dark-colored minerals), and  
438 epidote. The presence of muscovite could be an indicator of low weathering of initial  
439 sediments.

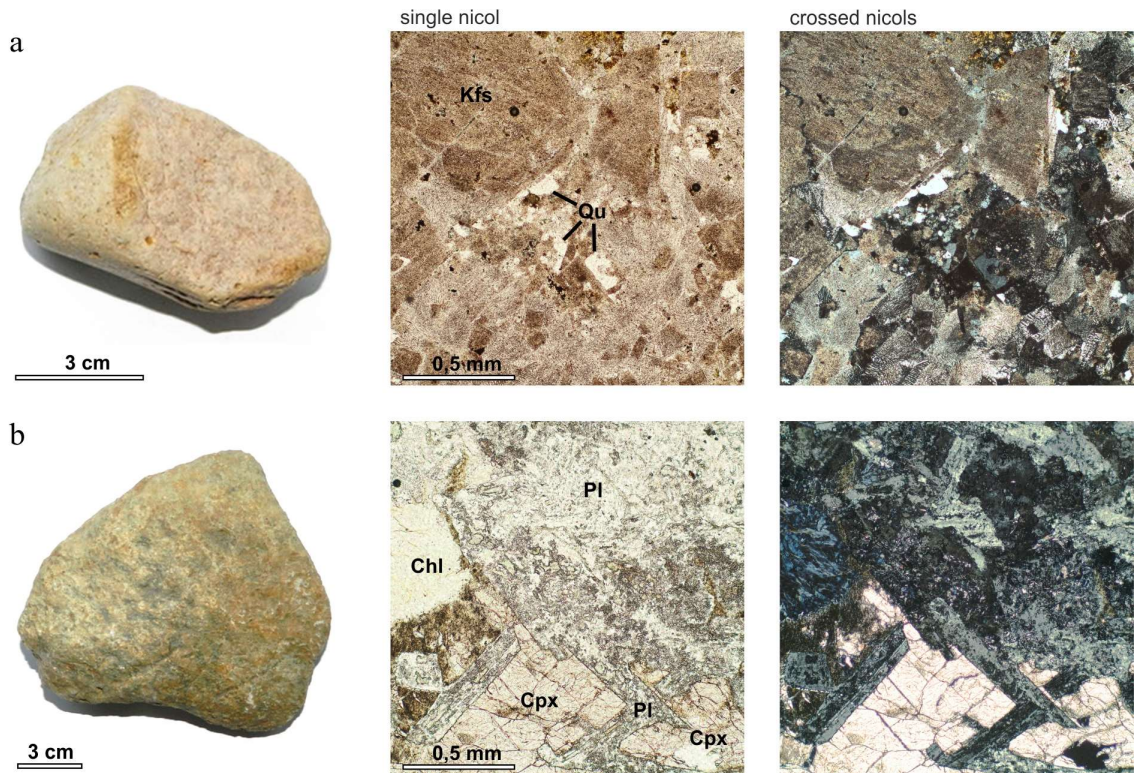
440 2) Pebbles and boulders of the second group of quartzitic and quartz sandstone  
441 (6 samples) feature angular forms. The textures are usually massive and vary from  
442 poorly to well sorted. The cement is predominantly quartz or quartz-  
443 hydromicaceous, sometimes with goethite. The grain size varies greatly, but  
444 medium-sized varieties prevail. More than 95% of grains are quartz and siliceous  
445 lithoclasts, while muscovite, feldspar, epidote, zircon, monazite, and opaque  
446 minerals are also present. The quartzitic sandstones show regenerative incrustations  
447 around the primary rounded quartz grains. The grain boundaries are most often  
448 irregular and frequently saw-shaped, which indicates a notable meta-genetic  
449 alternation. Late veins of the fine-grained quartz aggregate are also rather frequent.

450 3) The third group of samples was the least numerous yet the most  
451 informative. In this case, the first sample is a cobble of pinkish quartz trachyte-  
452 alkaline intermediate volcanic rock. Large pelletized phenocrysts of potassic  
453 feldspar (up to 1 cm) and rare fine quartz grains are distributed in the groundmass  
454 composed of pelletized potassic feldspar and quartz (Figure 8 a). Furthermore,  
455 quartz-feldspathic myrmekites are rather frequent. There are small quantities of  
456 plagioclase, dark-colored minerals that are substituted by aggregates of chlorite,  
457 epidote, and opaque mineral.

458 The second sample is dolerite with typical poikilitic texture (Figure 8 b)  
459 formed by large poikilite clinopyroxene crystals (3-4 mm in diameter) with tabular  
460 plagioclase (up to 1-1.5 mm). There are large, separate hypidomorphic crystals of  
461 basaltic hornblende (up to 2 mm), which are substituted by hydrous ferric oxides,  
462 titanite, and chlorite. The main groundmass contains plagioclase and significant  
463 amounts of chlorite, which is presumably a product of substitution of the volcanic  
464 glass or clinopyroxene microliths.

465 The third sample is zoisite-amphibolite (zoisite-actinolite) metasomatic rock.  
466 Light-green idiomorphic grains of amphibole prevail over hypidomorphic crystals  
467 and sheaf-like aggregates of zoisite. Anhedral segregations of titanite and opaque

468 ore minerals are also present. From a general chemical perspective, it can be  
 469 suggested that the most probable protolith for this rock was a dolerite-like rock.  
 470



471 **NEW** 3 cm  
 472 Fig. 8. (a) Sample N-10 – pinkish quartz trachyte, large inclusions of potassic feldspar (Kfs) with  
 473 fine quartz grains (Qu) in the quartz-feldspathic matrix; (b) sample N-14: greenish-brown  
 474 dolerite, large poikilitic clinopyroxene crystals (Cpx) with thin plagioclase crystals (Pl), in the  
 475 groundmass: plagioclase chlorite (Chl).  
 476

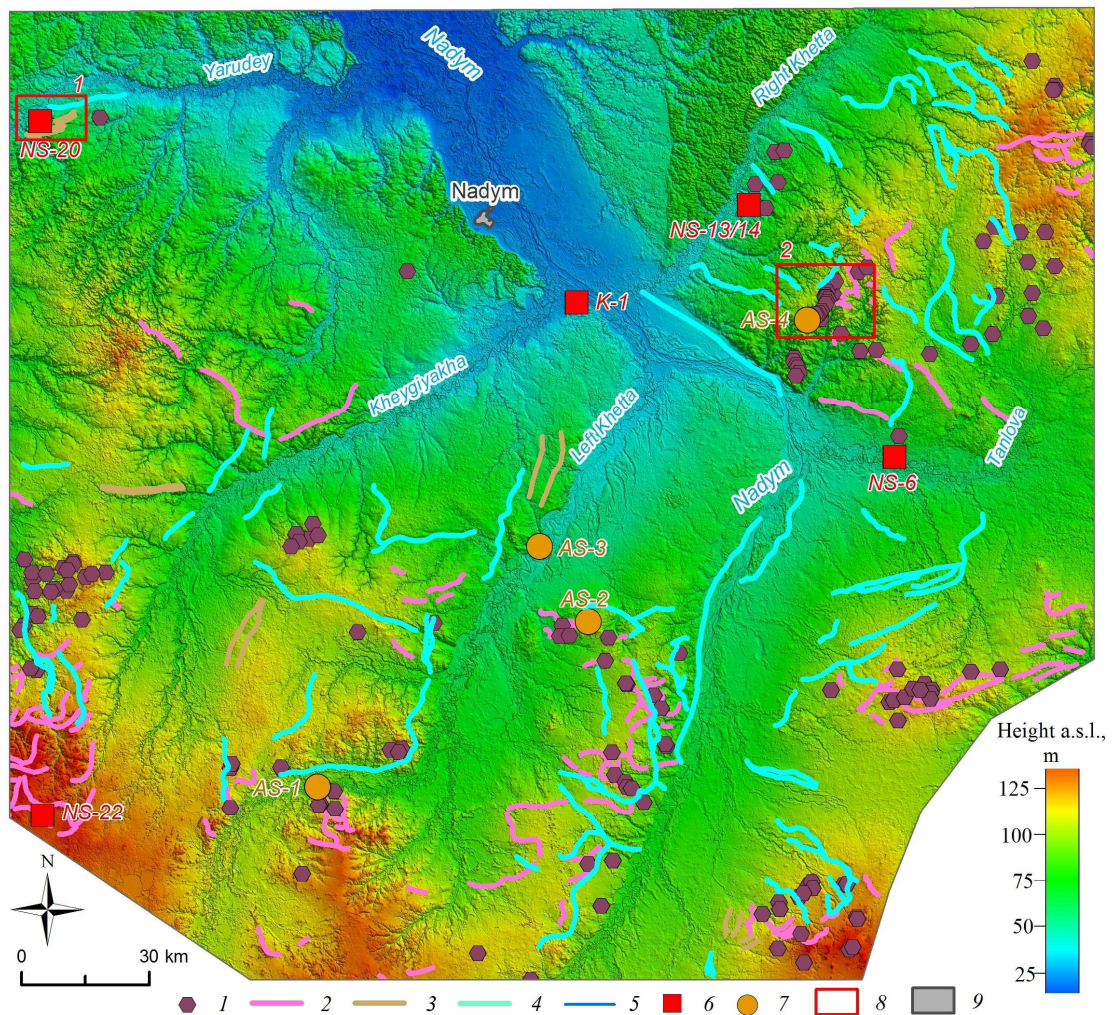
### 477 3.5. Geomorphological Analysis

478 The investigated area is in the zone of sparse northern taiga with extensive  
 479 peatlands. Therefore, the existing digital surface model (DSM), based on X-band  
 480 radar data with high penetration capacity, reflects in detail the terrain structure of  
 481 the territory. DEM mapping of the glacial ice and fluvio-glacial relief features was  
 482 performed using a site with an area of 54,117 km<sup>2</sup> as an example. Its boundaries run  
 483 along the watershed of the Nadym River and its tributaries. The summary mapping  
 484 results are shown in Table 4 and Figure 9.  
 485

486 Table 4  
 487 Remote mapping of the glacial and fluvio-glacial relief features in the Nadym River basin (mid  
 488 and lower courses)

Relief features	Number of identified objects	Total area/length, km
Kame-like hummocks	157	-
End moraines	122	851.3
Parallel ridges	16	157.2
Valley trains	103	1411.3

489



490  
491  
492  
493  
494  
495  
496

NEW

Fig. 9. Results of the glacial and fluvio-glacial relief interpretation in the middle course of the Nadym River (the background image is a synthesized digital terrain model based on DEM TanDEM-X, 26 m resolution): 1: kame-like hummocks; 2: moraines; 3: parallel ridges; 4: valley trains; 5: waterways; 6: studied and sampled locations; 7: additional locations based on Khlebnikov, 1954; Yevseyev, 1958; 8: areas of typically glacial landforms; 9: settlements

497  
498  
499

Based on the map obtained (Figure 9), it can be noted that the spread of the assumed glacial and fluvio-glacial relief features within the investigated area has two distinct patterns:

500  
501  
502  
503  
504  
505  
506  
507

- all identified features are to the south off the Yarudey and Right Khetta rivers, with individual objects found in the watershed between Yarudey and Kheygiyakha. In the southern and western parts, the diversity and density of the features are the highest (Tanlova and Right Khetta rivers watershed, left bank of the Nadym River in its middle course);
- all identified features are found at the heights from 40 m a.s.l. and higher; the density of objects significantly increases in the watershed areas above 70-75 m a.s.l.

508  
509  
510  
511  
512

The feature of the high elevation relief distribution is demonstrated by the statistical data about the selected kameform hills. Among the 157 point objects, 145 (92%) are above 75 m a.s.l., with 53 (34%) located within the narrow range of 95-104 m a.s.l. Below 75 m a.s.l., large objects occur individually and are poorly distinguished morphologically.



513 The network of extended (more than 850 km) end moraines that mark the final  
514 glacial massif positions is confidently recognized. They have different stretches  
515 (sub-latitudinal, north-western, etc.), which may indicate there was no single  
516 direction of the cover ice movement. In most cases, the moraines are confined to the  
517 watersheds, while they are often accompanied by other glacial forms (kames, [valley](#)  
518 [trains](#), etc). The chain of kame hills on the watershed of the Tanlova and Right  
519 Khetta Rivers are erosive remnants of the local moraine formations, i.e.  
520 morphologically they occupy an intermediate position between the individual  
521 moraines. On the watersheds, well-drained, dry areas of sands near kame ridges are  
522 often subjected to deflation and active redispersal.

523 Some of the individual objects are linear ridges (about 157 km total length).  
524 The linear ridge relief also has visible signs of erosion (scours, rills, subsidences)  
525 and in most cases can be traced as a specific linear landscape texture.

526 The valleys and rills of the melt glacial waters flow are more than 1,400 km  
527 long. The valleys are well expressed in the southern and eastern parts of the study  
528 area and are barely visible below 40 m asl. The network of valleys does not really  
529 match the modern watercourses; they can be located both in parallel at a small  
530 distance from the ancient valleys, or intersect them at right angles. The valleys and  
531 hollows of the ancient runoff are often associated with terminal formations. The  
532 preservation of valleys is one of the key signs of marine transgression absent in the  
533 middle course of the Nadym River since the last glaciation of the region.

534 For clarity, two sections of typically glacial landforms are highlighted on the  
535 map ([Figure 9](#)):

536 1. A site with a predominant linear ridge relief, located on the right bank of  
537 the Yarudey River (left tributary of the Nadym River), near the Nadym-Salekhard  
538 highway under construction ([Figure 10](#)). Four long, curved ridges reaching a height  
539 of 55 m a.s.l. are well-preserved (the difference in relative heights is 10-12 m). To  
540 the south of the ridges stands a section of hilly, presumably kame, relief. The ridges  
541 are complicated by thermokarst and erosion features.

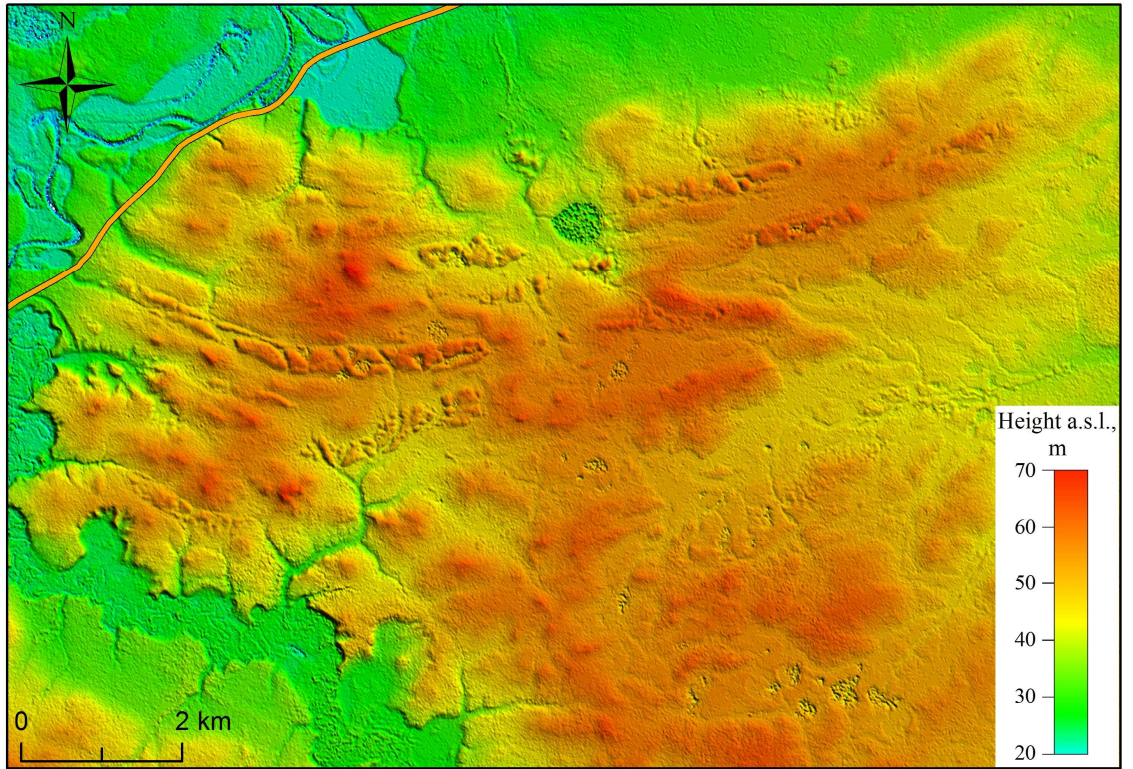
542 2. The kame hill concentration site on the right bank of the Nadym River,  
543 ([Figure 11](#)). The kames reach an absolute height of more than 100 m a.s.l. (difference  
544 in relative height up to 30 m). The kames are well preserved despite the destruction  
545 of individual features by the river erosion.

546

## 547 ***Discussion***

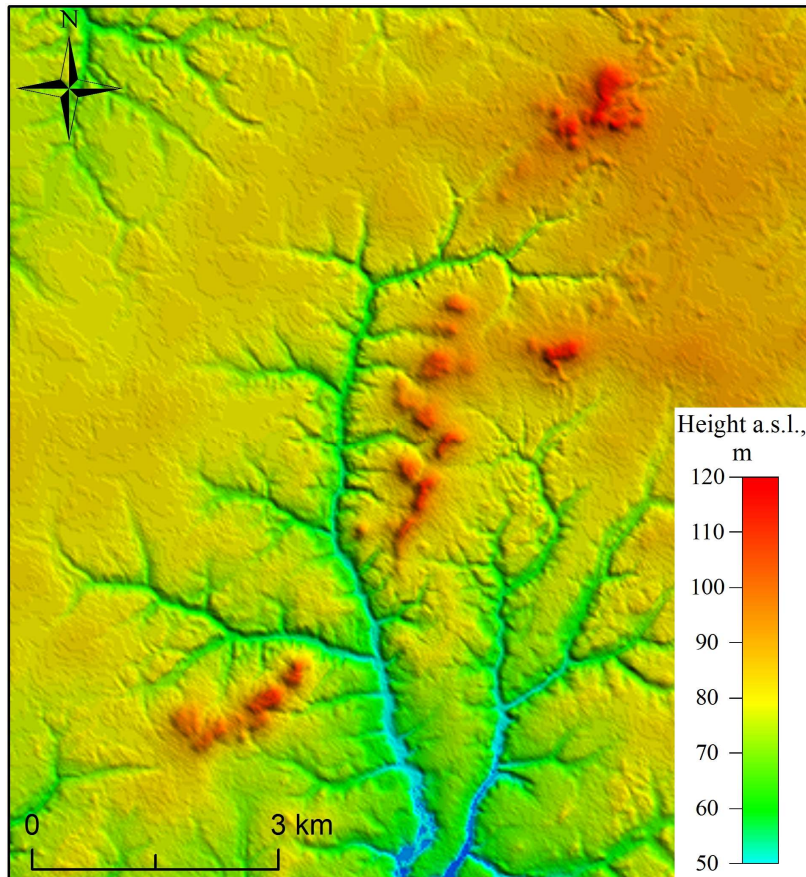
548 According to current viewpoints, the territory of the north of Western Siberia  
549 was exposed to several cover glaciations: Zyryanka (MIS 4), Taz (MIS 6) and  
550 Samarovo (MIS 8). Areas at the lower level (up to 40-45 m a.s.l.) could represent  
551 serial repeated marine transgressions in Kazantsev (MIS 5) and Karga (MIS 3) ages.  
552 The glaciation boundaries are presented in [Figure 12](#). [The correlation of the main](#)  
553 [palaeoenvironmental events in the Western Siberia with those on the East European](#)  
554 [Plain is presented in \[Figure 13\]\(#\). Directly within the boundaries of the investigated](#)  
555 [areas the boundaries of Taz \(MIS 6\) and possibly Zyryanka glaciation periods are](#)  
556 [identified \(\[Zemtsov, 1976\]\(#\); \[Babushkin, 1996\]\(#\)\).](#)

557



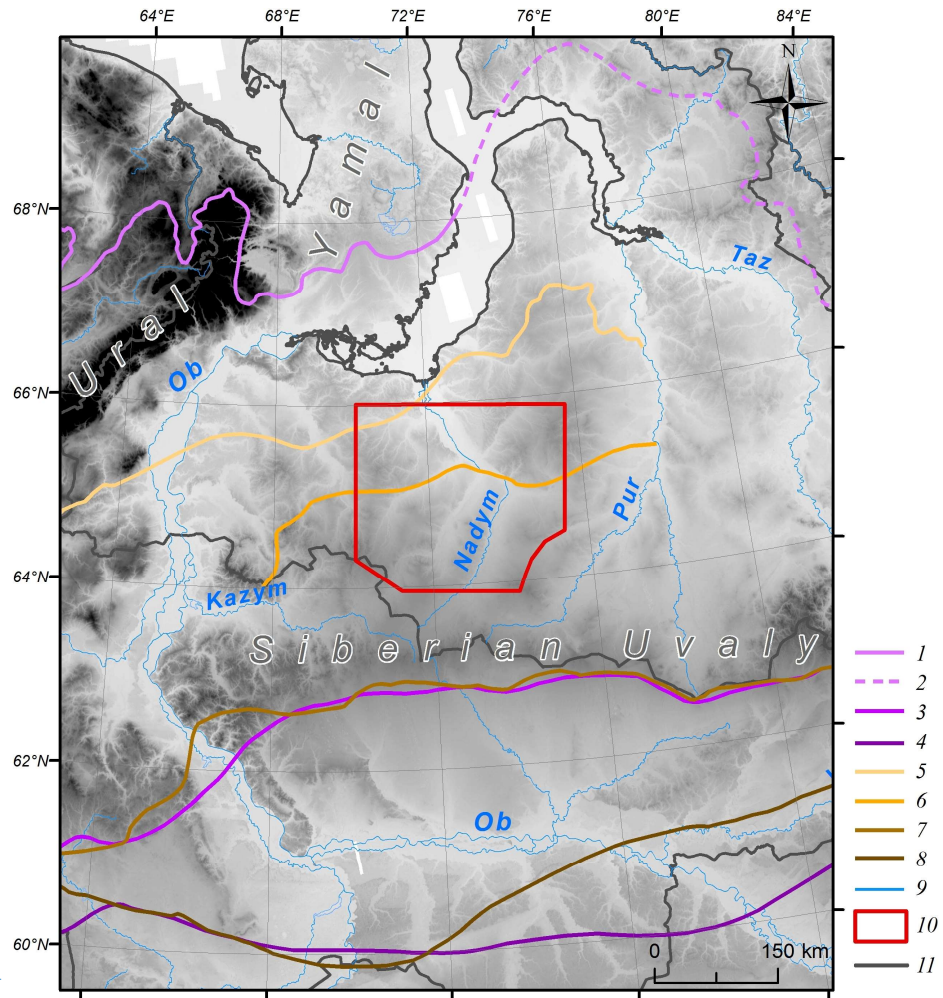
558 NEW — Nadym-Salekhard highway  
 559  
 560

Fig. 10. Parallel ridges, DEM TanDEM-X, 12 m / px.



561 NEW  
 562  
 563  
 564

Fig. 11. Kame-like features, DEM TanDEM-X, 26 m / px.



565  
566  
567  
568  
569  
570  
571

NEW

Fig. 12. 1-8: ice sheet boundaries (1: Zyryanka (Astakhov et al., 2016); 2: Zyryanka (assumed) (Astakhov et al., 2016); 3: Taz (Astakhov et al., 2016); 4: Samarovo (maximum) (Astakhov et al., 2016); 5: Zyryanka (Zemtsov, 1976; Babushkin, 1996); 6: Taz (second stage) (Zemtsov, 1976; Babushkin, 1996); 7: Taz (Zemtsov, 1976); 8: Samarovo (Zemtsov, 1976)); 9: water bodies; 10: study area; 11: administrative boundaries. Background: TanDEM-X 90m DEM ©DLR.

Age (Ma)	East-European Plain	MIS	Western Siberia
0	Holocene	1	Holocene
LATE	Valdai cold warm cold	2	Sartanian cold
		3	Karginian warm
		4	Ermakovian(Zyrian) cold
		5	Kazantsevo warm
MIDDLE	Mikulino warm	6	Tazovian cold
		7	Shirta warm
		8	Samarovo cold
		9	Tobolian warm
		10	
11	Likhvin warm		

572  
573  
574  
575  
576

Fig. 13. Palaeoenvironmental event successions on the East-European Plain (from Bolikhovskaya, 2004; Molodkov and Bolikhovskaya, 2010) and in Western Siberia (Interregional Stratigraphic Chart..., 2014).

577           The key natural feature of the glacial genesis of Quaternary strata in northern  
578 Western Siberia is the presence of wrecked rock: semi-rounded angular stones,  
579 gravel and large boulders with evident glacial [striation](#), carried over by the glacier  
580 from the territories outside the West Siberian Plain (Strelkov et al., 1965; Zemtsov,  
581 1976). The water-glacial sediments in the research area include well-washed grey  
582 sand characterized by poor chemical composition (the gravimetric concentration of  
583 SiO<sub>2</sub> is 94-97%) and also containing amendments of gravel and stones (Chekunova,  
584 1954; Groysman, 1954; Khlebnikov, 1954). The glacial sediments include unsorted  
585 coarse-grained sands with an abundance of pebbles, as well as moraine-like bodies  
586 of lumped clay, loam, and clay sand with gravel and large boulders. The petrographic  
587 composition of boulders and pebbles includes quartz, opal, sandstones, quartz  
588 porphyres, amphibolites, granitoids, gneises and trachites (Chekunova, 1954;  
589 Groysman, 1954; Khlebnikov, 1954). However, it was noted that interpreting the  
590 exact location of the origin of these rocks from the geological markers representing  
591 different territories is so far problematic.

592           The results of the study of the sections, in general, showed that the youngest  
593 of the discussed sediments are those of the second floodplain terrace (section NS-6,  
594 K-1). In the top part, it includes aeolian sand formed no later than the beginning of  
595 the Holocene (MIS 1), in the middle part there are floodplain series of alluvium, in  
596 the lower part there are river streams of grey oblique sand of the late MIS 3 – middle  
597 MIS 2.

598           The absolute age of the second floodplain terrace formation of the Nadym and  
599 Tanlova Rivers (sections K-1 and NS-6) correlates well with [radiocarbon and OSL](#)  
600 [datings of postglacial Pleistocene sediments throughout all the northern Western](#)  
601 [Siberia \(the age ranging from 42,000 to 25,000 years\) \(Astakhov and Nazarov,](#)  
602 [2010\)](#). On average, the age of the cover formation is between 20,000 and 12,000  
603 years (Astakhov, 2006; Zemtsov, 1976) Two types of glacial relief areas and  
604 extensive sandur surfaces were identified on the surface of the second floodplain  
605 terrace in the large-scale field studies on the left bank of the Left Kheta River  
606 (Vasilyev, 2007).

607           On the middle and upper topographical level, grey monoquartz sand in  
608 sections NS-20 and NS-22 was also found. Its age is similar: the beginning of MIS5.  
609 It can be suggested that during the Kazantsev interglacial period in the vast area of  
610 the Nadym River basin there were favorable conditions for the erosion of the  
611 previously accumulated sandy textured deposits and their transfer downstream the  
612 main rivers.

613           One of the most interesting points of research is the kameform hill on the left  
614 bank of the Right Khetta River (NS-13/14), the formation of its middle part  
615 corresponds to the Tobol interglacial period (MIS 9-11). It can be suggested that the  
616 sediments in the upper part of the hill are not younger than the Taz glaciation (MIS  
617 6), while the pebble layer formed during the degradation of the glacier reinforced  
618 the previous sediments and later was resistant to erosion, and was not covered by the  
619 waters of the Kazantsev and Karga transgressions

620           The results of the sand quartz grain morphology analysis confirmed the  
621 supposed genesis of the studied sections. [Thus, for sections NS-6 and K-1 it was](#)

622 shown that in the upper part of sections the sequence is: aeolian sediments, aluvial  
623 flood plain facies, and channel facies of coarse stratified sands. At the base of both  
624 sections, there are sediments in which, apart from typically river grains, a large  
625 number of various morphology grains are found. These are grains of varying degree  
626 of roundness, irregular shape with a smooth surface and smooth faces, often on their  
627 surface, there are various grooves and scratches formed under the strong mechanical  
628 impact, as well as conchoidal fractures. Their origin could be a result of freezing  
629 weathering and cryogenic transformation (Velichko and Timireva, 1995), as well as  
630 of high pressure applied to the grain surface (Immonen et al., 2014; Vos et al., 2014).  
631 Well-rounded ellipsoid and ball-shaped grains predominate in the top layer  
632 sediments. One can associate this distribution with materials coming from two  
633 different sources. One source could have been the former glacial sediments eroded  
634 by fluvial processes. This type of terrace structure corresponds well with the results  
635 of the study by Velichko et al. (2011) who analyzed sands with underlay peat  
636 deposits in the investigated region.

637 Quartz grains from sections NS-13/14 and NS-20 are often characterized by  
638 low rounding classes, multiple conchoidal fractures, sometimes even conchoidal  
639 systems, a deep-pitted surface, scratches, grooves, and cleavage surfaces. Such  
640 elements could be signs of processes that occur in glacial environments. Often, there  
641 are also signs of subsequent water treatment: separate crescentic depressions and  
642 smoothed sharp peaks of grains. It indicates the redeposition of the glacial grains by  
643 water flows. Along with the grains described above, there are also typical subaquatic  
644 grains: well-rounded with a fine-pitted surface, but their number is inferior to grains  
645 with glacial features.

646 Currently, we lack sufficient evidence to confirm the glacial genesis of these  
647 deposits. It is possible that the grains were exposed to the effects of glacial processes,  
648 with a final processing phase in their history that included subaquatic processes. In  
649 section NS-22, the grain morphology provides evidence that suggests the existence  
650 of a quiet subaquatic environment under which quartz grains underwent long-term  
651 treatment.

652 In general, the results of sand quartz grain morphoscopy and morphometry  
653 show that most quartz grains from all sections underwent complex multi-stage  
654 processing throughout their life.

655 The petrographic diversity of erratic boulders in West Siberia helps us  
656 distinguish two or three paleoglacial regions that combine several dozen distributed  
657 provinces. Each is characterized by a specific set of rocks and petrographic features.  
658 The first major generalization in this respect was made by Zemtsov (1976), who  
659 identified the guide boulders of the Ural region as ultramafic and mafic rocks of the  
660 Main (axial) Uralian zone, plagiogranites, and highly metamorphosed rocks  
661 (gneisses and shales). In the Central Siberian region, the prevailing boulders include  
662 dolerites and basalts of the Putorana Plateau, as well as various granitoids, quartzites,  
663 and Palaeozoic sandstones of the Taimyr Region. These studies were substantially  
664 [supplemented and detailed work](#) by Sukhorukova et al. (1987).

665 Despite their small quantity, the petrographic analysis of pebbles and boulders  
666 led to the following conclusions. First, high-silica alkaline effusive rocks (sample

667 N-10, quartz trachyte) are indicative of both the Northern Taimyr Province (Troitsky  
668 and Shumilova, 1973) and many moraines of the Ural paleoglacial region  
669 (Sukhorukova et al., 1987), but they are never found in the Putorana Plateau and the  
670 southmost regions. Moreover, there is only a small relative share of dolerites (sample  
671 N-14, dolerite) and other effusive mafic rocks, which is a property of Putorana and  
672 Nizhnyaya Tunguska regions. In contrast, there is no limestone that would be typical  
673 of the Central Siberian paleoglacial region (Kulyumbinsk and Sukhaya Tunguska  
674 distributive provinces according to Sukhorukova et al., 1987). **There is** no granite in  
675 the samples either, which is a property of the Northern Taimyr region.

676 Second, quartz and quartzite sandstones are typical for the Ural paleoglacial  
677 region, but their share is usually within a few per cent. Quartzitic sandstones also  
678 described as Palaeozoic were found 50 km north of Surgut within the tentative  
679 Central Siberian and Middle rock outwash zones (Sukhorukova et al., 1987). The  
680 source of the polymictic platy jointing sandstone could be the Palaeozoic bordering  
681 of the eastern slope of the Urals (Sukhorukova et al., 1987) or the Mesozoic  
682 sandstone of the West Siberian Plate.

683 In general, the samples have a significant proportion of terrigenous rocks  
684 (sandstones and siltstones) and low content of dolerites. On the one hand, this can  
685 be explained by the poor representativeness of the samples. Nevertheless, the key  
686 washout zone could be located further north than the Putorana Plateau in the Taimyr  
687 area. To substantiate this point of view, further research is planned to determine the  
688 trace element composition and absolute dating and to expand the sampling.

689 Despite the numerous features that make it possible to attribute the thickness  
690 of grey monomineral quartz sand (K-1, NS-6, NS-20) to fluvio-glacial sediments, and  
691 the upper pebble strata of section NS-13/14 to glacial sediments, the study did not  
692 find typical moraine-like formations of lumped clay, loam and clay sand with gravel  
693 and large boulders in this territory. However, detailed descriptions of this type of  
694 sediment can be found in some references (Strelkov S.A. et al., 1965; Zemtsov,  
695 1976; Sukhorukova et al., 1987; Babushkin, 1996 etc.).

696 Thus, in the middle course of the Right Khetta River at Point 70 (Khlebnikov,  
697 1954) 2.5 m deep there is a **20 m-thick until** of densely clumped loam with  
698 interlayers of mica enriched sand (**the layers are up to 25 cm thick**) (section AS-1,  
699 Figure 9). The color of the loam is **brown**, small glitter mica is visible, and **angular**  
700 debris (granite) are found, up to 25 cm in diameter. In the right part of the section  
701 upstream, stripping exposed a layer of fine-grained sand. Below 15 m it is followed  
702 by an interlayer of gravel-pebble rock. The prominent colluvium slope is covered by  
703 loam crushed stone, and a cluster of gravel-pebble rock is also found on the **towpath**.

704 **The huge kame moraine was described in the watershed of Nadym and Left**  
705 **Khetta rivers (point 2368) (section AS-2, Figure 9) (Khlebnikov, 1954).** It has a wide  
706 extension and rises up to 25-30 m above the surrounding plain. The ridge part of the  
707 range is convex and consists of individual peaks separated by meso ridges. On the  
708 surface of the ridge, the congestion of pebble and gravel is found. The gravel-pebble  
709 coarse-grained well-washed and leached sand is traced down to the depth of 1.2 m.

710 Two esker-like linear elevations and a small kameform hill were discovered  
711 in the lower course of the Right Khetta River at well No. 18 (Khlebnikov, 1954) at

712 1.8 m depth in the gravel-pebble horizon with a total depth of 17.6 m (section AS-3,  
713 Figure 9). The diameters of the pebbles are between 0.5 and 3-4 cm. The pebbles are  
714 not rounded and consist mainly of quartz and sandstone.

715 The moraine hills in the upper part of the Big Huhu River (right tributary of  
716 the Nadym River) have a north-west and a north-east orientation. The length reaches  
717 6-7 km, and the relative height varies from 15 to 60 m. (Chekunova, 1954; Yevseyev,  
718 1958) morphologically, the steep slopes of the hills have individual smoothed tops  
719 separated by small saddles. The upper layer of the hills to a depth of 1-2 m is peeled  
720 loam with abundant pebble rock. The pebbles are weak and poorly rounded, and  
721 their diameters do not exceed 2-4 cm. Petrographic composition in one of the  
722 sections reveals (so-called point 367 (Chekunova, 1954)): silica, clay shale, arkoses  
723 sandstones, breccia of clay-quartz rocks and limonite. The results of manual drilling  
724 at some small hills (Yevseyev, 1958; Andreev, 1960) showed that they are folded  
725 with permafrost sediments. The total ice content as determined visually is not less  
726 than 30%. As an example, well No. 10 (Yevseyev, 1958), where light grey clay with  
727 yellowish color, light, porous, with alevrite interlayers is found at a depth of 1.4-  
728 10.7 m, has a wavy and horizontal lamination (section AS-4, Figure 9). Clay  
729 thickness is underlayed with grey clay fine-grained sands with poor sorting and  
730 admixture of gravel grains, quartz, and silicon pebbles.

731 Data from both our studies and previous field studies are in good  
732 correspondence to the results of the analyses with the Tandem-X Digital Terrain  
733 Models. These models revealed that despite the plain origin of the territory, the high  
734 salinity and dominance of erosion processes, various glacial and fluvio-glacial relief  
735 features preserved to various degrees (kameform hills, proximal moraines, and linear  
736 elevations, glacial meltwaters etc.) are evident.

737 A linear-oriented relief caused by a glacial impact in northern Western Siberia  
738 is highlighted on the Map of Quaternary Formations in Russia, 1:2,500,000 scale  
739 (Astakhov et al., 2016). At the same time, linear features and glacial remains are  
740 identified on geological maps of larger scales (Babushkin, 1996).

741 Nowadays, due to the increasing availability of initial DTM data, remote  
742 mapping of glacial relief features become the standard method across the world  
743 (Clark et al. 2004; Glasser et al. 2008; Sharpe et al. 2010; [Atkinson et al. 2014](#);  
744 [Norris et al. 2017](#)). Based on modern spatial data, a detailed map for the British Isles  
745 Territory and Coastal Zone (BRITICE-2) is available for digital study and analysis,  
746 and was updated ([Clark et al., 2018](#)). The remote features of most forms of glacial  
747 relief for various natural conditions are described in detail and offer numerous  
748 evidence that can be used as standards for remote sensing data interpretation,  
749 including the entire north area of Western Siberia.

750

### 751 *Conclusions*

752 Our results showed high efficiency of simultaneous application of field  
753 ground and remote methods even with limited raw site rocks. Sediments were  
754 identified, which can be immediately attributed to fluvio-glacial (lower part of  
755 section K-1 and NS-6, section NS-20) and glacial (upper layer of section NS-13/14)  
756 origins. Traces of glacial treatment were also found as landforms in certain areas

757 such as kameform hills, proximal moraines, linear-bed elevations, and depressions  
758 of melt glacial water runoffs. Due to low organic substance content, sparse lichen-  
759 pine trees are formed over the fluvio-glacial sediments on the low-fertile podzolic  
760 soils. It is a characteristic landscape feature of the leaching soil condition for the  
761 north taiga in Western Siberia. At the same time, the moraine-like layers of  
762 aggregated clay, loam and clay sand with gravel and large boulders that could not  
763 be found in field studies are widely described [in sources](#) previously unpublished  
764 (particularly the Left Khetta and in the upper reaches of the [Big Huhu River](#)).

765 Thus, the development history of the Nadym River lower stream area provides  
766 evidence that periods of cover glaciations occurred here in the Pleistocene. At the  
767 same time, it is difficult to say whether it was a single glacier with a common front,  
768 or whether there were several separate centers of ice accumulation. The available  
769 data, especially the structure and functional characteristics of the relief, appear to  
770 favor the second option, at least in the late Pleistocene. In the early periods, traces  
771 of larger glaciation may represent the vast lake-alluvial plains and flood plains,  
772 reaching a maximum area in the basin of the Nadym, Pur and Taz rivers. In this case,  
773 they can be considered as the latest erosion formations but preserved a characteristic  
774 structure inherited by modern landscapes.

775

#### 776 *Acknowledgements*

777 The authors thank the Terrasar-X (DLR) research team for providing the  
778 [TanDEM DTM for research \(DEM\\_GEOL1378\)](#). We also thank the anonymous  
779 [reviewers whose comments and suggestions helped improve and clarify this](#)  
780 [manuscript](#).

781 This study was funded by the RFBR and the [Yamal-Nenets Autonomous](#)  
782 [District, project number 19-45-890008](#). The investigation is under a public  
783 assignment by the Institute of Geology and Mineralogy, [SB, RAS](#).

784

#### 785 *References*

- 786 Alyavdin F.A., and Mokin N.P.: Geological map. 1rd ed. Scale 1:1,000,000. Ministry of Geology  
787 and Subsoil Protection of the USSR, Map Q-43 (Novyy Port). Gosgeoltekhizdat, Moscow,  
788 1957.
- 789 Andreev Yu.F.: About the relationship of linear-ridge topography with tectonic structures in the  
790 north of Western Siberia (in the field of permafrost development). *Geologiya i geokhimiya*.  
791 *Geology and geochemistry*, 3(IX), 76–94, 1960.
- 792 Astakhov, V.I.: On chronostratigraphic units of the Upper Pleistocene in Siberia, *Geologiya i*  
793 *geofizika*, 47(11), 1207–1220, 2006.
- 794 [Astakhov, V., and Nazarov, D.: Correlation of Upper Pleistocene sediments in northern West](#)  
795 [Siberia. \*Quaternary Science Reviews\*, 29\(25-26\), 3615–3629., 2010.](#)
- 796 Astakhov, V., Shkatova, V., Zastrozhnov, A. and Chuyko, M.: Glacio-morphological Map of the  
797 Russian Federation, *Quaternary International*, 420, 4–14, 2016.
- 798 Atkinson, N., Utting, D., and Pawley, S.: Landform signature of the Laurentide and Cordilleran  
799 ice sheets across Alberta during the last glaciation. *Canadian Journal of Earth Sciences*,  
800 51(12), 1067-1083, doi: 10.1139/cjes-2014-0112, 2014
- 801 Babushkin, A.E.: Quaternary map. 2rd ed. Scale 1:1,000,000. Russian Federation Committee on  
802 Geology and Mining (Roskomnedra), Map Q-42,43 (Salekhard). St. Petersburg: VSEGEI  
803 Cartographic Factory, 1996.



- 804 Bolshiyarov, D.Yu.: Passive Glaciation of the Arctic and Antarctic Regions. AANII, Saint  
805 Petersburg, 296 p, 2006.
- 806 Chekunova, V.S.: Geological and geomorphological survey of a part of the lower reaches of the  
807 Nadym River basin and parts of the right bank of the Nadym Ob River. VSEGEI, Leningrad,  
808 1954.
- 809 Clark, C, Evans, D, Khatwa, A., Bradwell, T., Jordan, C., Marsh, S., Mitchell, W. and Bateman,  
810 M.: Map and GIS database of glacial landforms and features related to the last British ice  
811 sheet. *Boreas*, 33, 359–375, 2004.
- 812 Clark, C., Ely, J., Greenwood, S., Hughes, A., Meehan, R., Barr, I., Bateman, M., Bradwell, T.,  
813 Doole, J., Evans, D., Jordan, C., Monteys, X., Pellicer, X. and Sheehy, M.: BRITICE Glacial  
814 Map, version 2: a map and GIS database of glacial landforms of the last British–Irish Ice  
815 Sheet. *Boreas*, 47, 11–27, 2018.
- 816 Bolikhovskaya, N.S.: Paleoenvironments and climato-stratigraphy of the loess-paleosol formation  
817 of Northern Eurasia. *Loess inForm*, 4, 11–36, 2004.
- 818 Faibusovich, Ya.E. and Abakumova, L.A.: Map of Pliocene-Quaternary formations. 3rd ed. Scale  
819 1:1,000,000. Federal Agency for Subsoil Use (Rosnedra), Map Q-43 (New Urengoy). St.  
820 Petersburg: VSEGEI Cartographic Factory, 2015.
- 821 Fredin, O., Rubensdotter L., Welden, A., Larsen, E. and Lysa, A.: Distribution of ice marginal  
822 moraines in NW Russian, *Journal of Maps*, 8(3), 236–241, 2012. doi:  
823 10.1080/17445647.2012.708536
- 824 Glasser, N., Jansson, K., Harrison, S., and Kleman, J.: The glacial geology and Pleistocene history  
825 of South America between 38,8S and 56,8S. *Quaternary Science Reviews*, 27, 365–390,  
826 2008.
- 827 Grosvald, M.G.: Eurasian Hydrospheric Catastrophes and Glaciations of the Arctic Region,  
828 Nauchny Mir, Moscow, 1999.
- 829 Groysman, Ya.M.: Geological survey of the Haigi-Yakh River basin (Long-Yugan). VSEGEI,  
830 Leningrad, 1954.
- 831 Generalov, P.P.: Upper Pleistocene of the lower course of the Ob River In: Collection of scientific  
832 papers of the West Siberian Scientific and Research Geological Prospecting Petroleum  
833 Institute, Tyumen, 56–77, 1986.
- 834 Immonen, N., Strand, K., Huusko, A., and Lunkka, J.P.: Imprint of late Pleistocene continental  
835 processes visible in ice-rafted grains from the central Arctic ocean. *Quaternary Science*  
836 *Reviews* 92, 133–139, 2014.
- 837 Interregional stratigraphic chart of the Quaternary of the territory of the Russian Federation.  
838 Interdepartmental Stratigraphic Committee, VSEGEI, St. Petersburg, 2014.
- 839 Kalinska-Nartisa E., Woronko B., and Ning W.: Microtextural inheritance on quartz sand grains  
840 from Pleistocene periglacial environments of the Mazovian Lowland, Central Poland.  
841 *Permafrost and Periglacial Processes* 28, 741–756, 2017.
- 842 Khabakov, A.V.: On roundness indexes of pebble, *Sovetskaya Geologiya*, 10, 98–99, 1946.
- 843 Khlebnikov, V.I.: Geological and geomorphological survey of a part of the middle reaches of the  
844 Nadym river basin. VSEGEI, Leningrad, 1954.
- 845 Krinsley, D.H., and Doornkamp, J.C.: Atlas of quartz sand surface textures. 2nd edition.  
846 Cambridge, Cambridge University Press, 102, 2011.
- 847 Kind, N.V.: Late Quaternary Geochronology According to Isotope Data. Nauka, Moscow, 1974.
- 848 Lazukov, G.I.: Antopogen of the northern part of Western Siberia (Paleogeography), Moscow, 127  
849 p, 1972.
- 850 Maslennikov, V.V.: Regional Geo-Ecological Mapping at Scale of 1:1000000 Within the North  
851 End of Tyumen Oblast. Labytnangi, 1998.
- 852 Molodkov, A.: The Late Pleistocene palaeoenvironmental evolution in Northern Eurasia through  
853 the prism of the mollusc shell-based ESR dating evidence. *Quaternary International*, (in  
854 press.), 2020.

- 855 Molodkov, A.: Cross-check of the dating results obtained by ESR and IR-OSL methods:  
856 implication for the Pleistocene palaeoenvironmental reconstructions. *Quat. Geochronol.*, 10,  
857 188–194, 2012.
- 858 Molodkov, A., and Bolikhovskaya, N.: Climato-chronostratigraphic framework of Pleistocene  
859 terrestrial and marine deposits of Northern Eurasia based on pollen, electron spin resonance,  
860 and infrared optically stimulated luminescence analyses. *Est. J. Earth Sci.* 59(1), 49–62,  
861 2010.
- 862 Molodkov, A., and Bitinas, A.: Sedimentary record and luminescence chronology of the  
863 Lateglacial and Holocene aeolian sediments in Lithuania. *Boreas*, 35 (2), 244–254, 2006.
- 864 Norris, S. L., Margold, M., and Froese, D.G.: Glacial landforms of northwest Saskatchewan.  
865 *Journal of Maps*, 13, 600–607, doi:10.1080/17445647.2017.1342212, 2017.
- 866 Rukhin, L.B.: *Fundamentals of Lithology. Doctrine of Sedimentary Rocks.* Nedra, Leningrad,  
867 1969.
- 868 Rusakov, A., Sedov, S., Sheinkman, V., Dobrynin, D., Zinovyev, E., Trofimova, S. and  
869 Levchenko, S.: Late Pleistocene paleosols in the extra-glacial regions of Northwestern  
870 Eurasia: Pedogenesis, post-pedogenic transformation, paleoenvironmental inferences.  
871 *Quaternary International*. 501, 174–192, doi:10.1016/j.quaint.2018.03.020, 2018.
- 872 Sharpe, J., Sharpe, D., and Harris J.: A flowline map of glaciated Canada based on remote sensing  
873 data. *Canadian Journal of Earth Sciences*, 47, 89–101, 2010.
- 874 Sedov, S., Rusakov, A., Sheinkman, V., and Korkka, M.: MIS3 paleosols in the center-north of  
875 Eastern Europe and Western Siberia: Reductomorphic pedogenesis conditioned by  
876 permafrost? *Catena*, 146, 38–47, doi:10.1016/j.catena.2016.03.022, 2016
- 877 Sheinkman, V., Sedov, S., Shumilovskikh, L., Korkina, E., Korokin, S., Zinovyev, E. and Golyeva,  
878 A.: First results from the Late Pleistocene paleosols in northern Western Siberia:  
879 Implications for pedogenesis and landscape evolution at the end of MIS3. *Quaternary*  
880 *International*, 418, 132–146, doi:10.1016/j.quaint.2015.12.095, 2016.
- 881 Sizikova, A.O. and Zykina V.S.: The dynamics of the Late Pleistocene loess formation, Lozhok  
882 section, Ob loess Plateau, SW Siberia. *Quaternary International*, 365, 4–14, 2015.
- 883 Strelkov S.A., Saks V.N., Arkhipov S.A., and Volkova V.S.: The problem of the Quaternary  
884 glaciations of Siberia. The main problems of the study of the Quaternary period, Nauka,  
885 Moscow, 188–205, 1965.
- 886 Svendsen, J., Alexahderson, H., Astakhov, V., Demidov, I., Dowdeswell, Ju., Funder, S., Gataulin,  
887 V., Henriksen, M., Hjort, H., Houmark-Nielsen, M., Hubberten, H.-W., Ingolfsson,  
888 O., Jakobsson, M., Kjar, K., Larsen, E., Lokrantz, H., Lunkka, Ju. P., Lysa, A., Mangerud, J.,  
889 Matiouchkov, A., Murray, A., Moller, P., Niessen, F., Nikolskaya, O., Polyak, L., Saarnisto,  
890 M., Siegert, Ch., Siegert, M., Spielhagen, R. and Stein, R.: Late Quaternary ice sheet history  
891 of Northern Eurasia. *Quaternary Science Reviews*, 23 (11–13), 1229–1271, 2004.
- 892 Sukhorukova, S.S., Kostyuk M.A., Podsova, L.L., Babushkon A.E., Zolnikov, I.D., Abramova,  
893 S.A. and Goncharov, S.V.: *Moraines and Dynamics of Glaciation in Western Siberia.* Works  
894 of Institute of Geology and Geochemistry of the Siberian Branch of the USSR Academy of  
895 Sciences, Issue 672. Nauka, Novosibirsk, 1987.
- 896 Troitskiy, S.L. and Shumilova, E.V.: *Stratigraphy and Mineralogical-Petrographic Peculiarities of*  
897 *Quaternary Deposits in the Vorontsov Yar Stratum in the Lower Course of the Yenisei River.*  
898 *In: Lithology and Conditions of Formation of the Quaternary Deposits of the Northern*  
899 *Eurasia, Institute of Geology and Geochemistry of the Siberian Branch of the USSR*  
900 *Academy of Sciences, Novosibirsk, 5–37, 1974.*
- 901 Vasilyev, S.V.: *Forest and Bog Landscapes of Western Siberia.* Izdatelstvo NTL, Tomsk, 2007.
- 902 Velichko, A.A. and Timireva S.N.: Morphoscopy and morphometry of quartz grains from loess  
903 and buried soil layers, *GeoJournal*, 36(2/3), 143–149, 1995.
- 904 Velichko, A.A., Timireva, S.N., Kremenetski, K.V., McDonald, G.M. and Smith, L.C.: West  
905 Siberian Plain as a late glacial desert, *Quaternary International*, 237 (1–2), 45–53, 2011.
- 906 Velichko, A.A.: Current state of conceptions on continental glaciers of the Earth. *Bulletin of the*

- 907 Academy of Sciences of the USSR, Geographical Series, 3, 21–34, 1987.
- 908 Velichko, A.A., Kononov, V.M. and Faustova M.A.: The last glaciation of Earth: size and volume  
909 of ice-sheets, *Quaternary International*, 41 (42), 43–51, 1997.
- 910 Vos, K., Vandenberghe, N. and Elesen, J.: Surface textural analysis of quartz grains by scanning  
911 electron microscopy (SEM): From sample preparation to environmental interpretation,  
912 *Earth-Science Reviews*, 128, 93–104, 2014.
- 913 Woronko, B.: Frost weathering versus glacial grinding in the micromorphology of quartz sand  
914 grains: Process and geological implications. *Sedimentary Geology*, 335, 103–119, 2016.
- 915 Zemtsov, A.A.: *Geomorphology of the West Siberian Plain (Northern and Central Parts)*,  
916 Publishing house of the Tomsk State University, Tomsk, 1976.
- 917 Yevseyev, G.P., and Reynin, I.V.: *Geological structure and geomorphology of the Tanlova, Right  
918 Khetta, and Big Huhu basins (right tributaries of the middle segment of the Nadym river).*  
919 VNIGRI, Leningrad, 1958.
- 920

921 *Annexes*

922

923 Annex 1. Bulk content of chemical elements

Sampling depth, m	Sample No	Bulk content, %							
		SiO <sub>2</sub>	Al <sub>2</sub> O <sub>3</sub>	Fe <sub>2</sub> O <sub>3</sub>	K <sub>2</sub> O	Na <sub>2</sub> O	P <sub>2</sub> O <sub>5</sub>	CaO	TiO <sub>2</sub>
K-1									
0.1	S1	87.65	5.27	0.95	1.66	1.00	0.03	0.51	0.64
0.35	S2	88.09	5.14	1.89	1.14	0.56	0.05	0.32	0.53
1	S3	89.49	4.93	1.20	1.52	0.75	0.04	0.41	0.41
1.8	S4	92.97	3.35	0.61	1.32	0.51	0.02	0.27	0.21
2.3	S5	90.71	4.21	0.92	1.35	0.64	0.03	0.38	0.39
3	S6	98.02	0.88	0.30	0.25	0.07	0.01	0.10	0.10
4	S7	98.39	0.69	0.25	0.20	<0.05	0.01	0.08	0.08
NS-6									
0.3	S1	90.60	6.20	0.87	0.91	0.63	0.08	0.28	0.37
0.7	S2	91.85	4.57	0.74	1.47	0.58	0.01	0.41	0.37
1.4	S3	93.22	3.92	0.51	1.15	0.57	0.01	0.31	0.25
3.2	S4	92.37	4.05	0.75	1.38	0.62	0.02	0.43	0.35
4	S5	90.32	5.39	0.98	1.74	0.62	0.02	0.46	0.47
4.2	S6	97.33	1.54	0.26	0.15	0.45	0.00	0.18	0.08
4.6	S7	89.79	5.86	0.95	1.80	0.65	0.03	0.63	0.35
5	S8	96.65	1.88	0.28	0.42	0.49	0.01	0.20	0.11
7.4	S9	97.29	1.46	0.24	0.25	0.48	0.01	0.16	0.07
9.2	S10	97.78	1.19	0.21	0.07	0.45	0.01	0.17	0.07
NS-13/14									
1.1	S1	97.72	1.43	0.21	0.00	0.43	0.00	0.14	0.10
3.1	S2	91.00	1.26	5.62	0.00	0.63	1.28	0.16	0.07
3.5	S3	96.58	1.22	1.14	0.15	0.56	0.12	0.18	0.11
4	S4	98.14	0.99	0.15	0.00	0.48	0.00	0.15	0.07
4.3	S5	96.25	1.18	1.58	0.07	0.47	0.06	0.16	0.24
4.75	S6	92.75	1.23	5.08	0.01	0.64	0.02	0.18	0.12
5	S7	98.34	0.89	0.17	0.00	0.43	0.00	0.13	0.09
NS-20									
1.5	S1	95.61	1.79	0.39	0.48	0.08	0.02	0.08	0.44
3.7	S2	95.59	1.83	0.21	0.68	0.09	0.01	0.07	0.16
6.5	S3	97.12	1.14	0.19	0.39	0.09	0.01	0.07	0.10
9.5	S4	94.30	2.31	0.31	0.84	0.10	0.02	0.07	0.38
16.45	S5	97.26	0.93	0.22	0.22	0.05	0.01	0.07	0.20
NS-22									
1.1	S1	96.49	1.53	0.32	0.61	0.17	0.01	0.11	0.17

924

925

926 Annex 2

927 Spearman's coefficients of correlation

	SiO <sub>2</sub>	TiO <sub>2</sub>	Al <sub>2</sub> O <sub>3</sub>	Fe <sub>2</sub> O <sub>3</sub>	MnO	MgO	CaO	Na <sub>2</sub> O	K <sub>2</sub> O	P <sub>2</sub> O <sub>5</sub>	BaO
SiO <sub>2</sub>	1	-1	-1	-0.89	-0.84	-0.76	-0.89	-0.89	-0.79	-0.81	-0.62
TiO <sub>2</sub>	-1	1	1	0.89	0.94	0.75	0.89	0.89	0.79	0.83	0.73
Al <sub>2</sub> O <sub>3</sub>	-1	1	1	0.89	0.94	0.78	0.89	0.89	0.79	0.84	0.73
Fe <sub>2</sub> O <sub>3</sub>	-0.89	0.89	0.89	1	0.93	0.95	0.75	0.75	0.61	0.97	0.61
MnO	-0.84	0.94	0.94	0.93	1	0.86	0.85	0.85	0.76	0.91	0.78
MgO	-0.76	0.78	0.78	0.95	0.86	1	0.67	0.67	0.52	0.99	0.54
CaO	-0.89	0.89	0.89	0.75	0.85	0.67	1	1	0.96	0.71	0.91
Na <sub>2</sub> O	-0.89	0.89	0.89	0.75	0.85	0.67	1	1	0.96	0.71	0.91
K <sub>2</sub> O	-0.79	0.79	0.79	0.61	0.76	0.52	0.96	0.96	1	0.56	0.96
P <sub>2</sub> O <sub>5</sub>	-0.81	0.83	0.84	0.97	0.91	0.99	0.71	0.71	0.56	1	0.59
BaO	-0.62	0.73	0.73	0.61	0.78	0.54	0.91	0.91	0.96	0.59	1

928 Significance level  $p < 0.05$

929

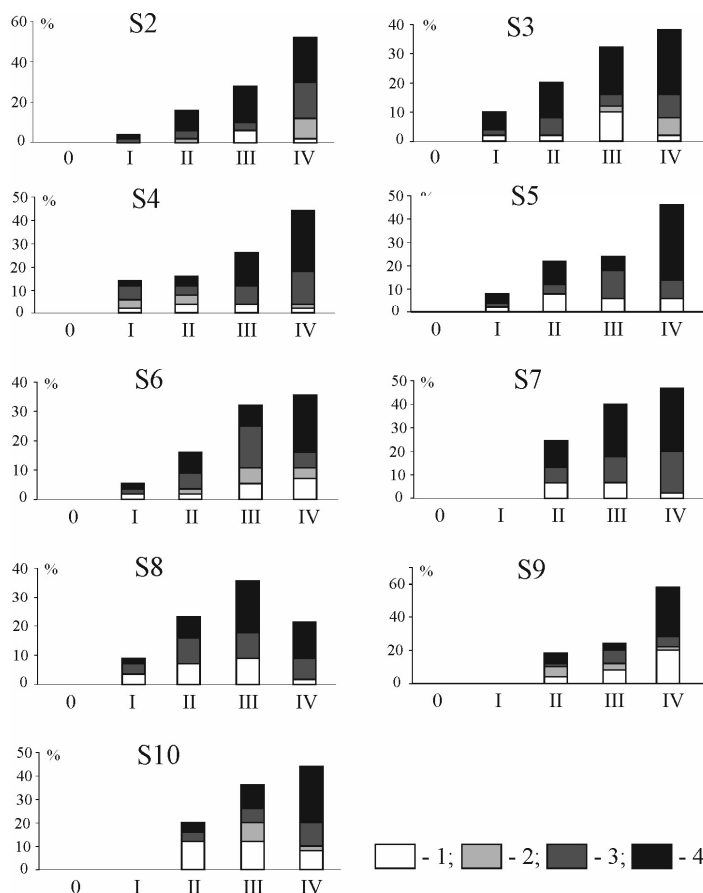
930

Sampling depth	Sample	Fraction size (mm) / Content (%)					
		Silt and clay	Very fine sand	Fine sand	Medium grained sand	Coarse Sand	Very coarse sand
<b>K-1</b>		<b>&lt;0.09</b>	<b>0.125-0.09</b>	<b>0.25-0.125</b>	<b>0.5-0.25</b>	<b>1-0.5</b>	<b>&gt;1</b>
0.1	S1	31.7	29.2	28.7	9.5	0.7	0.1
0.35	S2	18.7	12.5	32.1	32.2	4.2	0.3
1	S3	18.9	32.3	35.6	11.9	1.2	0.1
1.8	S4	5.9	20.1	56.7	16.4	0.9	0.0
2.3	S5	5.6	13.1	59.9	19.8	1.6	0.0
3	S6	0.6	0.4	1.8	71.5	23.7	1.9
4	S7	0.4	0.5	4.2	46.3	46.9	1.7
<b>NS-6</b>		<b>&lt;0.075</b>	<b>0.10-0.075</b>	<b>0.25-0.10</b>	<b>0.5-0.25</b>	<b>1-0.5</b>	<b>&gt;1</b>
0.3	S1	11.0	6.6	52.7	26.9	2.8	0.0
0.7	S2	0.8	6.8	70.8	18.7	0.4	1.9
1.4	S3	2.0	8.8	65.8	21.2	1.3	0.5
3.2	S4	3.6	8.4	72.8	15.2	0.0	0.0
4	S5	29.9	14.9	50.2	5.1	0.0	0.0
4.2	S6	2.8	0.0	29.4	61.9	5.9	0.0
4.6	S7	26.2	21.1	51.1	1.6	0.0	0.0
5	S8	0.0	0.0	41.1	55.0	3.9	0.0
7.4	S9	1.1	0.1	29.2	52.1	17.4	0.0
9.2	S10	0.5	0.0	29.4	57.5	12.6	0.0
<b>NS-13/14</b>		<b>&lt;0.075</b>	<b>0.10-0.075</b>	<b>0.25-0.10</b>	<b>0.5-0.25</b>	<b>1-0.5</b>	<b>&gt;1</b>
1.1	S1	0.0	0.0	0.6	37.4	58.0	4.0
3.1	S2	8.0	0.0	0.3	36.6	54.2	0.9
3.5	S3	5.9	0.0	10.6	59.9	23.6	0.0
4	S4	0.0	0.0	7.1	62.9	30.0	0.0
4.3	S5	24.4	1.2	15.3	40.9	18.0	0.1
4.75	S6	1.9	0.0	6.5	53.5	37.5	0.6
5	S7	0.0	0.0	8.0	61.5	30.6	0.0
<b>NS-20</b>		<b>&lt;0.09</b>	<b>0.125-0.09</b>	<b>0.25-0.125</b>	<b>0.5-0.25</b>	<b>1-0.5</b>	<b>&gt;1</b>
1.5	S1	0.0	2.2	62.1	21.9	1.3	12.5
3.7	S2	0.0	4.3	72.0	23.0	0.5	0.2
6.5	S3	0.0	4.4	55.8	38.5	1.1	0.3
9.5	S4	0.0	9.3	70.7	16.0	1.5	2.4
16.45	S5	0.0	0.9	56.8	37.6	4.0	0.6
<b>NS-22</b>		<b>&lt;0.09</b>	<b>0.125-0.09</b>	<b>0.25-0.125</b>	<b>0.5-0.25</b>	<b>1-0.5</b>	<b>&gt;1</b>
1.1	S1	0.0	1.4	53.3	44.3	0.9	0.1

932

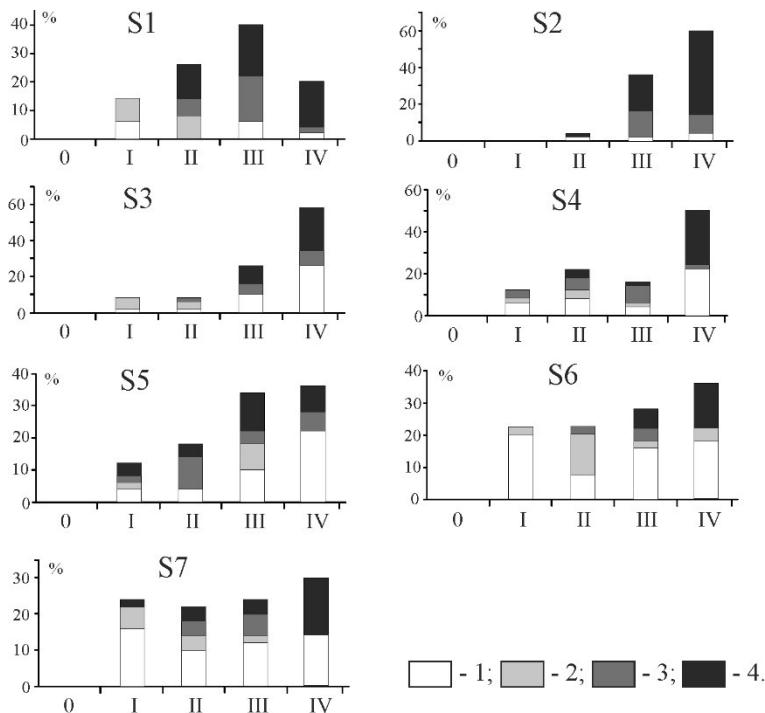
933

934



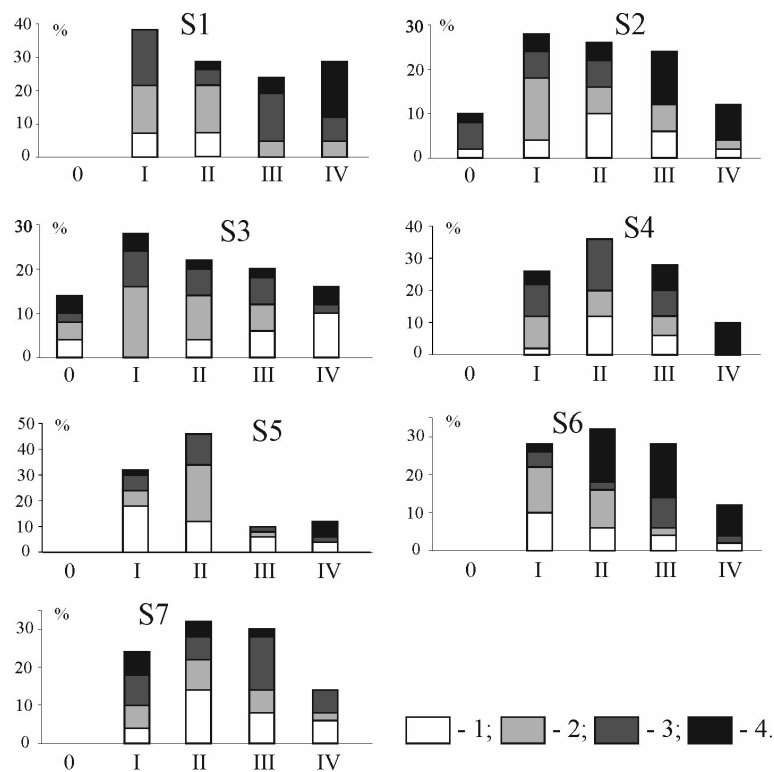
935  
936  
937  
938  
939  
940

Annex 4. Distribution of quartz sand grains from section NS-6 by roundness and dullness. 1:glossy; 2:quater-matte; 3:half-matte; 4: matte; 0, I, II, III, IV are grades of roundness according to Khabakov (1946) scale.

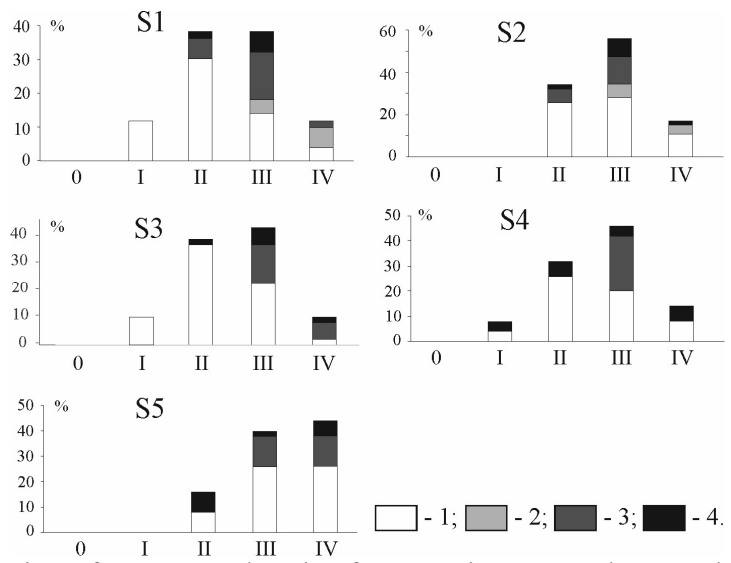


941  
942  
943  
944

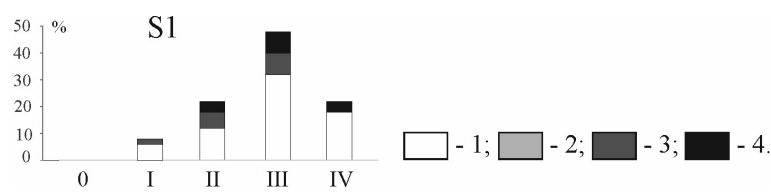
Annex 5. Distribution of quartz sand grains from section NS-6 by roundness and dullness. 1:glossy; 2:quater-matte; 3:half-matte; 4: matte; 0, I, II, III, IV are grades of roundness according to Khabakov (1946) scale.



945  
946  
947  
948  
949  
Annex 6. Distribution of quartz sand grains from section NS-13/14 by roundness and dullness.  
1:glossy; 2:quater-matte; 3:half-matte; 4: matte; 0, I, II, III, IV are grades of roundness according  
to Khabakov (1946) scale.

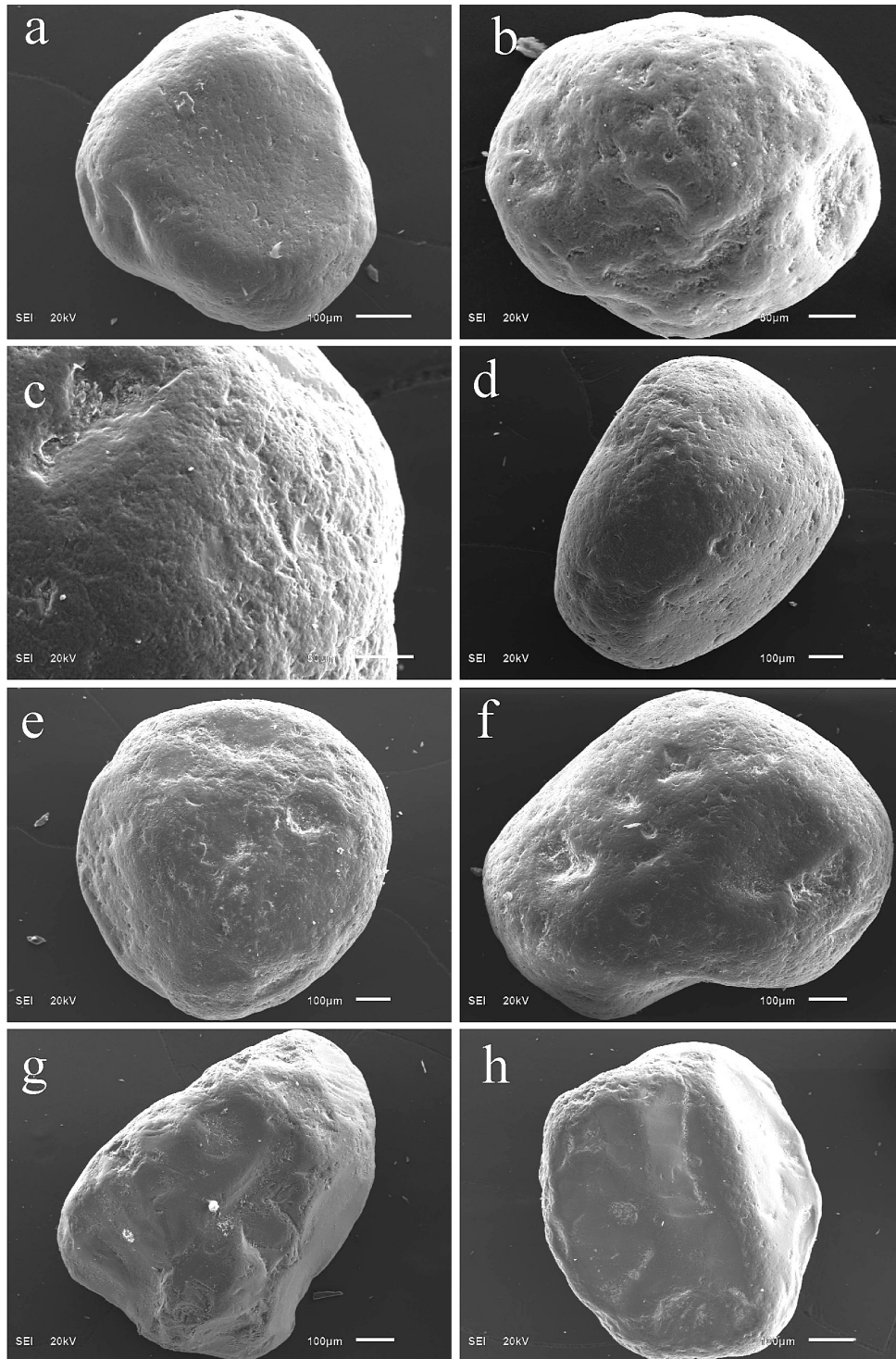


950  
951  
952  
953  
954  
955  
Annex 7. Distribution of quartz sand grains from section NS-20 by roundness and dullness.  
1:glossy; 2:quater-matte; 3:half-matte; 4: matte; 0, I, II, III, IV are grades of roundness according  
to Khabakov (1946) scale.



956  
957  
958  
959  
Annex 8. Distribution of quartz sand grains from section NS-22 by roundness and dullness.  
1:glossy; 2:quater-matte; 3:half-matte; 4: matte; 0, I, II, III, IV are grades of roundness according  
to Khabakov (1946) scale.





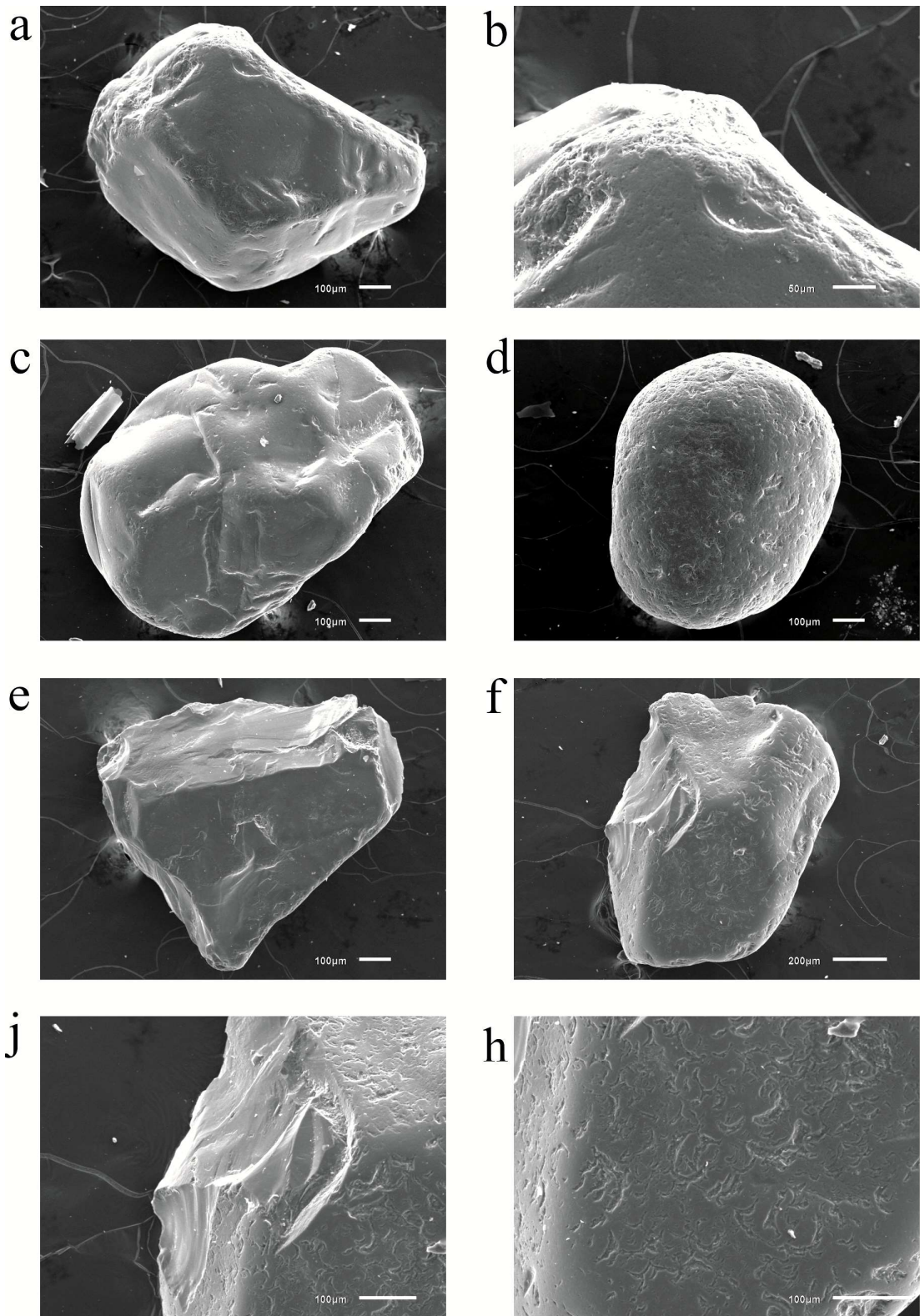
961  
 962  
 963  
 964  
 965  
 966  
 967  
 968  
 969  
 970  
 971  
 972  
 973

Annex 9. SEM photos of quartz grains, section NS-6.

Aeolian sediments: (a): dull grain with a micro-pitted surface and individual crescent-shaped depressions, (b): matte grain with a micro-pitted surface and traces of previous subaquatic treatment.

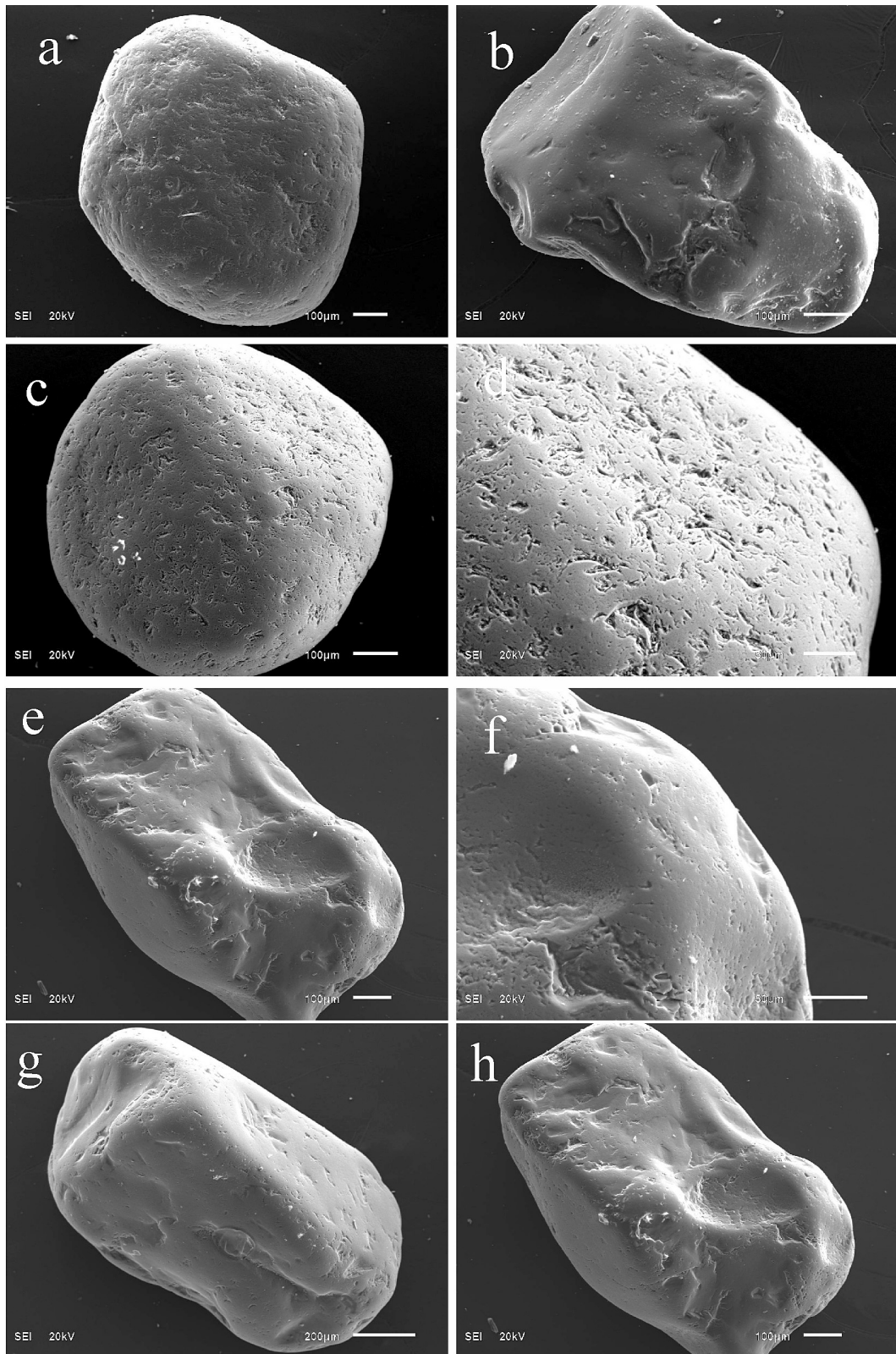
Floodplain sediments: (c): half-matte grain with V-shaped depressions, forming a fine-pitted surface, and with micro-pits, (d): half-matte grain with V-shaped depressions and fine-pitted.

Fluvial deposits: (e): glossy grain with a fine-pitted surface; (f): half-matte grain with a fine-pitted surface and separate V-shaped depressions; (g): glossy grain with fine-pits in the protruding parts of the grain; (h): glossy grain with presedimentation fractures, with the surface subjected to aquatic processes, as expressed by the shape of V-shaped depressions.



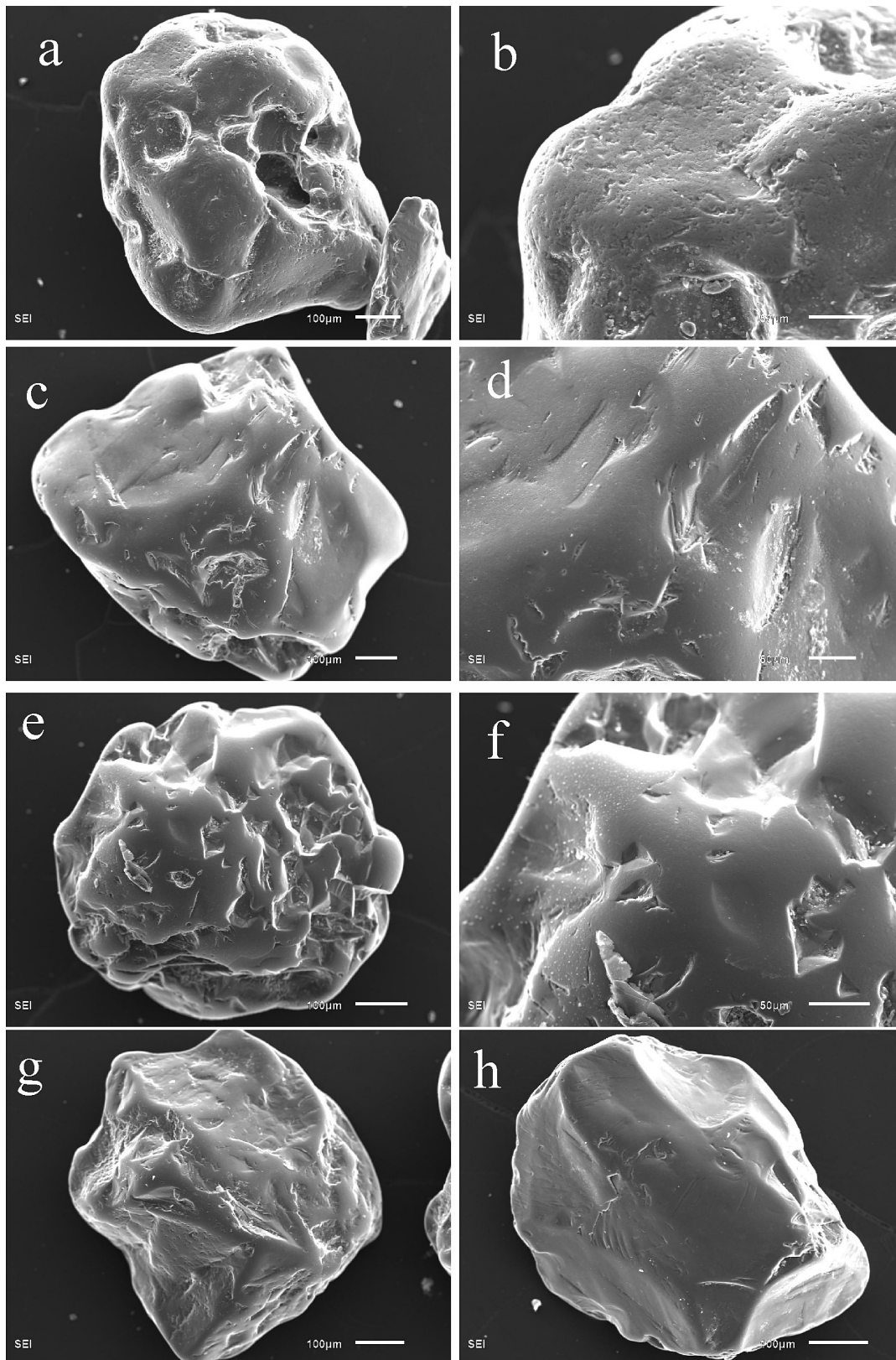
975  
 976  
 977  
 978  
 979  
 980  
 981  
 982

Annex 10. SEM photos of quartz grains from S7 section K-1: (a): glossy grain with a smooth surface and flat faces; the faces feature crescentic pits, grain tops feature fine pits; (b): fine-pitted surface of grain 'a'; (c): glossy grain with a smooth surface and sparse fine pits; (d): half-matte grain with fine-pitted surface and crescent pits; (e): glossy grain with flat faces and no evident texture; (f): glossy grain with post-sedimentation conchoidal fractures and crescentic pits; (j): conchoidal fracture of grain 'e'; (h): crescentic texture of grain 'e'.



983  
 984  
 985  
 986  
 987  
 988  
 989  
 990  
 991  
 992

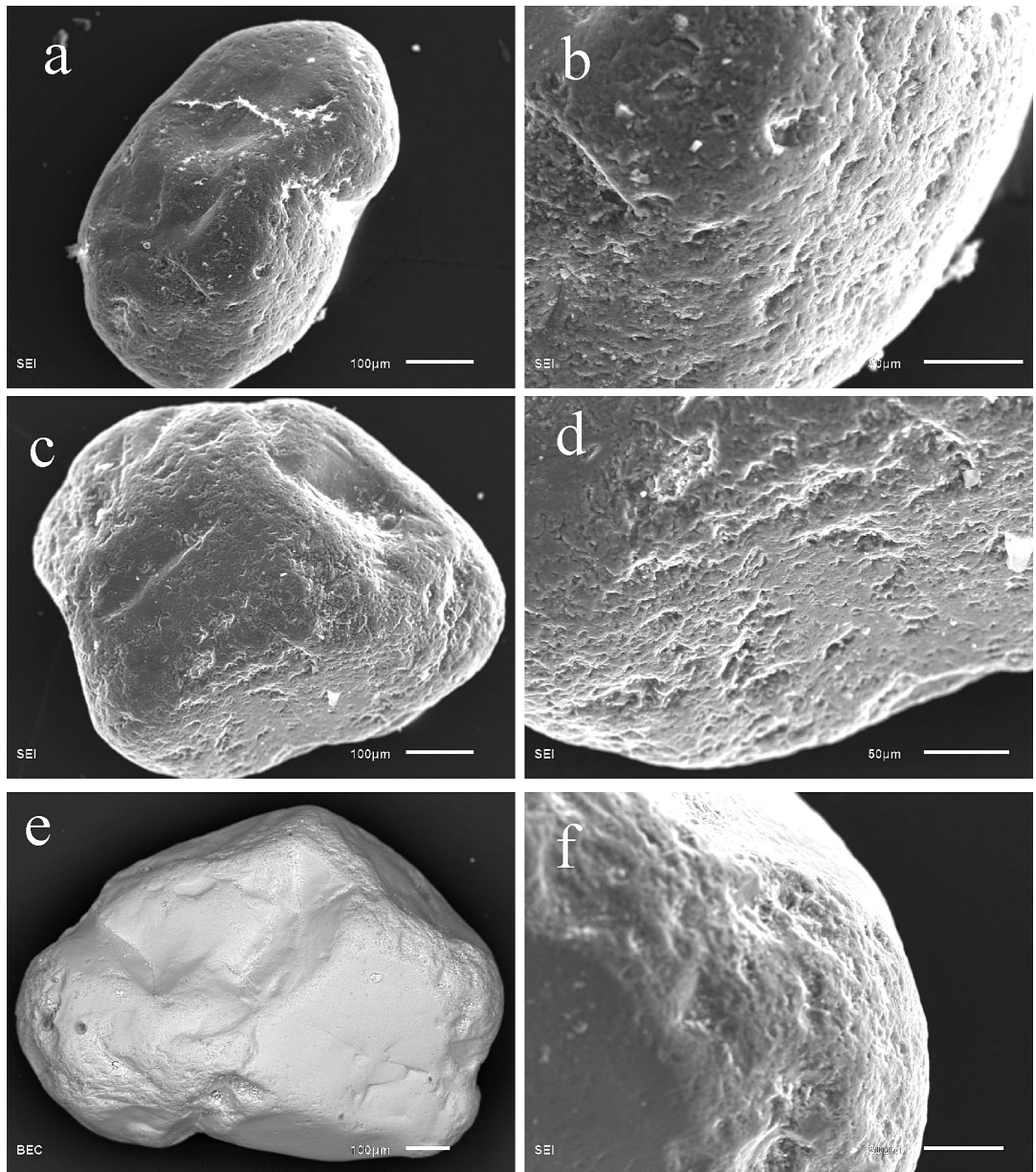
Annex 11. SEM photos of quartz grains from the section NS-13/14: (a) - glossy grain with fine-pitted and crescent and V-depressions; (b): glossy grain of irregular shape with chips and separate V-shaped **recesses**; (c), (d): half-matte grain with a crescentic texture and micropits; (e), (f): glossy grain with chips, V-shapes, and micro-pits on the protruding parts of the grain; (g): half-matte grain of irregular shape with a fine-pitted texture in the protruding parts of the grain; (h): glossy grain with a conchoidal fracture, V-shapes and fine-pits on the protruding parts of the grain.



994  
 995  
 996  
 997  
 998  
 999  
 1000  
 1001

Annex 12. SEM photos of quartz grains from the section NS-20.

(a), (b): matte cavernous grain with a micro-pitted surface and individual crescentic and V-shaped percussions, (c), (d): glossy grain with a smooth surface, grooves, and individual micro-pits, (e), (f): glossy grain with deep groove and single V-shaped percussions, (g): glossy grain of irregular shape with separate V-shaped percussions and a deep-pits, (h): glossy grain with presedimental conchoidal fractures and scratches.



1002  
 1003  
 1004  
 1005  
 1006  
 1007

Annex 13. SEM photos of quartz grains from the section NS-22.  
 (a), (b): glossy grain with a fine-pitted surface, (c), (d): glossy grain with a fine-pitted surface,  
 (e), (f): glossy grain with fine-pits on the protruding parts of the grain.